Optical Pumping and Magnetic Resonance

James Dragan

Lab Partner: Stefan Evans

Physics Department, Stony Brook University, Stony Brook, NY 11794.

(Dated: October 4, 2013)

We optically pump electrons in Rb^{85} to the $5^2S_{1/2}$, F=2, m_f=+2 state and in Rb^{87} to the $5^2S1/2$, F=3, m_f=+3 using the D_1 line $\lambda = 795$ nm, emitted by a Rb Lamp, which becomes σ^+ polarized due to a linear polarizer and a quarter-wave plate. We verify the pumping using an RF signal and stimulated emission to populate the next lower m_f level and observe the transmitted light read by a photodiode. We show that this transition is achieved in both isotopes. Using the absorption frequency we determine the Earths Magnetic field B_{Earth}, along the quantization axis z. The presence of this field splits the degenerate states in the hyperfine structure in absence of an external B field, by using theoretical values for g_F. We go onto determining the effects of power broadening the absorption dip. Lastly we measure Landẽg-factor, g_F in both isotopes from measuring an applied B field from Maxwells coils and the corresponding resonance frequency.

1. INTRODUCTION

Optical Pumping is a method first developed by Alfred Kastler[1] (who was awarded the Nobel Prize in 1966), that has become a widely used technique in experimental physics ever since. Optical pumping is a process in which electromagnetic radiation is used to pump electrons into a well-defined quantum state. The process by which this happens is dependent on the atomic structure of the sample and the properties of the radiation. The utilization of polarization and the selection rules for m leads to being able to pump the electrons into a dark state where there are no magnetic sublevels, m_f, to excite to. This can be used even when there is an m_f level to excite to and then the experimenter has a well-defined two-level system. The first thing one must account for is the atomic structure of the atomic sample.

1.1. Fine Structure

When an electron undergoes orbital motion, there is an associated orbital magnetic moment defined as $\vec{\mu} = I\vec{A}$ where $I = -e(\omega/2\pi)$ and $\vec{A} = \pi\vec{r}^2$. Rewriting ω in terms of the angular momentum L we find that

$$|\vec{\mu}| = \frac{-e\hbar}{2m}\hat{l} = \frac{-e\hbar}{2m}\sqrt{L(L+1)} \ , \tag{1}$$

where $\sqrt{L(L+1)}$ are the eigenvalues of the $\hat{L}$ operator and $\frac{e\hbar}{2m} = \mu_B = 9.27 \times 10^{-24} JT^{-1}$ is the Bohr magneton.

In the presence of an external field, the magnetic moment will undergo a precession due to the cross product of the two terms, resulting n a torque vector. Defining the fields axis along the quantization axis $\vec{L}_z$ one finds that the frequency of precession is the Larmor frequency:

$$\omega_L = \gamma B_0 \ . \tag{2}$$

Here $\gamma = \mu_B/\hbar$ is the gyromagnetic ratio. As stated we have defined the quantization axis to be $\vec{l_z}$. It is important to notice that $|L_z| < |\vec{L}|$. This means that the magnetic moment will never completely align with the field and thus it will always precess as described above.

Our next step is to account for the spin of the electron by which S=1/2 and m_s = -1/2, 1/2. It is shown that the resutling spin magnetic moment is[3]

$$\vec{\mu}_s = -g_s\frac{e}{2m}\vec{S} \ . \tag{3}$$

The Landé g-factor for spin, g_s, was theorized by Dirac to be 2, and then shown through Quantum Electrodynamics to be equal to 2.0023. As an aside, the motivation to measure g_F in this experiment is due to the fact that this number is disputed and g_F depends upon this value.

Next we must change our reference frame to the electron, e^-, which sees a nucleus precessing around itself. Because the nucleus is charged, for reasons discussed in later sections, the rotating charge produces a magnetic field. Using the Biot-Savart Law we find

$$\vec{B}_l = \frac{Ze^2\mu_0}{4\pi m r^3}\vec{l} \ . \tag{4}$$

The electrons spin magnetic moment interacts with this field through the relation

$$H_{FS} = \frac{Ze^2\mu_0}{8\pi m^2 r^2}(S \cdot L) \tag{5}$$

where $(S \cdot L)$ is given by the relation

$$J^2 = L^2 + 2L \cdot S + S^2 \ . \tag{6}$$

Rearranging the terms, we find

$$L \cdot S = \frac{1}{2}(J^2 + L^2 + S^2) = \frac{\hbar^2}{2}[J(J+1) - L(L+1) - S(S+1)] \ . \tag{7}$$

The full expression for the fine structure correction to the Hamiltonian is given by[3]

$$H_{FS} = \frac{E_g\alpha^2}{5}\left(\frac{1}{J+1/2}\right) \ . \tag{8}$$

If the atom had no angular momentum from the nucleus then this would hold enough information to fully describe the energy levels. In the case of this experiment we must take into account the spin of the nucleus.

1.2. Hyperfine Structure

Due to the spin of the nucleus, I = 3/2 in ^{87}Rb and I = 5/2 in ^{85}Rb, I and J couple to give our grand angular momentum quantum number $F = |\vec{F}| = |\vec{I} + \vec{J}|$. Looking at the nucleus' magnetic moment we see

$$\vec{\mu}_I = +g_I\frac{\mu_N}{\hbar}\vec{I} \ , \tag{9}$$

where g_I is the Landé g-factor for the nucleus' spin, $|\vec{I}| = \hbar\sqrt{I(I+1)}$, and $\mu_N = \frac{e\hbar}{2M} = \frac{\mu_B}{1836}$. The hyperfine perturbation to the Hamiltonian is given as follows:

$$H_{HFS} = -\vec{\mu}_I \cdot \vec{B}_J \tag{10}$$

where $\vec{B}_J$ is given by

$$\vec{B}_J = \frac{\vec{J}}{\sqrt{J(J+1)}} \ . \tag{11}$$

Thus

$$H_{HFS} = \frac{g_I \mu_N}{\hbar} B_j \frac{1}{\sqrt{J(J+1)}} (\vec{I} \cdot \vec{J}) \ . \tag{12}$$

We solve for $(\vec{I} \cdot \vec{J})$ in the same procedure as Eq (1.6) by defining the total atomic angular momentum number $\vec{F} = \vec{I} + \vec{J}$. Where $|\vec{F}| = \hbar\sqrt{F(F+1)}$ and F has values $F = |I - J|, .., |I + J|$ of integer steps. For each hyperfine level, there are 2F+1 magnetic sublevels, m_F. Solving for $(\vec{I} \cdot \vec{J})$ we find

$$(I \cdot J) = \frac{1}{2}[F(F+1) - I(I+1) - J(J+1)] \tag{13}$$

This gives us our full Hamiltonian for the hyperfine structure:

$$H_{HFS} = \frac{g_I \mu_N B_J}{2\sqrt{J(J+1)}}[F(F+1) - I(I+1) - J(J+1)] \ . \tag{14}$$

This is the full form for our hyperfine structure which we can now use to map out the energy levels of Rubidium.

1.3. Energy Levels of ^{85}Rb and ^{87}Rb

In this experiment we use naturally occurring Rubidium which comes in two isotopes, ^{85}Rb (72% abundance and nuclear spin quantum number I=5/2) and ^{87}Rb (28% abundance and nuclear spin quantum number I=3/2)[2]. Alkali Atoms are defined by having a positively charged core with a single valence electron, in our case occupying the 5s orbital. The electron shell of orbitals $[(1s^2)(2s^2)(2p^6)(3s^2)(3p^6)(4s^2)(3d^{10})(4p^6)]$ are all filled making this Rb^+ core spherically symmetric with a total angular momentum of L_c=0, spin orbital angular momentum of S_c=0. The LS-coupled angular momentum quantum number $\vec{J_c}$=$|J_c|$=$|\vec{L_c} + \vec{S_c}|$=0 where J is defined quantum mechanically to take values of increasing integers between $|L - S|$ to $|L + S|$.

Because the ion core does not contribute any total angular momentum, all the momentum quantum numbers come from the valence electrons. Considering the first electronic ground state,

with ionization energy 4.177eV or 296.81nm, in Rubidium $(5s)^2S_{1/2}$ we see that n=5, l=0, S=1/2, L=0 and therefore J = 1/2. Since J takes on only one value there is no fine structure in the $(5s)^2S_{1/2}$ state. For the first excited state, $(5p)^2P$,however there is fine structure splitting. We find that n=5, l =1, S = 1/2, L=1 and therefore J = 1/2, 3/2 which gives two fine structure levels of $(5p)^2P_{1/2}$ and $(5p)^2P_{3/2}$. The spin orbit coupling energy term is given by Eq. (8).

Using this equation we find that the $(5p)^2P_{1/2}$ is lower than the $(5p)^2P_{3/2}$ state. The energy to couple $(5s)^2S_{1/2}$ to $(5p)^2P_{1/2}$ is given as λ = 795 nm which is referred to as the D_1 line. The energy to couple $(5s)^2S_{1/2}$ to $(5p)^2P_{3/2}$ is given as λ = 780 nm which is referred to as D2 line[2,3]. In this experiment, both the D_1 and D_2 line are produced by the Rb Lamp, but we filter out the D_2 line so that only the D_1 line is incident on the atoms. It should also be noted that the lifetime of these excited states are extremely small, $\approx 10^{-8}s$ which is instantaneous with respect to how fast the photodiode can detect changes in the input power.

If we account for the nucleus, and its spin quantum number then we find even finer splittings in energy spectra. Looking at the ^{85}Rb isotope, $I = 5/2$, we find splittings in both fine structures. In the ground state $5^2S_{1/2}$ the degeneracy is split into two hyperfine levels F = 2, F =3. For the $5^2P_{1/2}$ state we find F = 2, 3 whereas for the $5^2P_{3/2}$ state F = 1, 2, 3, 4. Looking at the ^{87}Rb isotope with $I = 3/2$ we find that the ground state $5^2S_{1/2}$ is split to F = 1 and F = 2. In the two excited states we find that $5^2P_{1/2}$ is split into F = 1 and F = 2, while the $5^2P_{3/2}$ state has F = 0, 1, 2, 3.

As stated for each hyperfine F level, there are $2F + 1$ m_F sublevels if the degeneracy is lifted. For F = 1 there are 3 m_F levels corresponding to m_F = -1, 0, +1. For F = 2, m_F = -2, -1, 0, +1, +2. For F = 3, m_F = -3, -2, -1, 0, +1, +2, +3 and for F = 4, m_F = -4, -3, -2, -1, 0, +1, +2, +3, +4. A diagram of the energy structure for each isotope in the $5^2S_{1/2}$ and $5^2P_{1/2}$ state is shown. These are the corresponding ground state and excited state excited from the D_1 line.

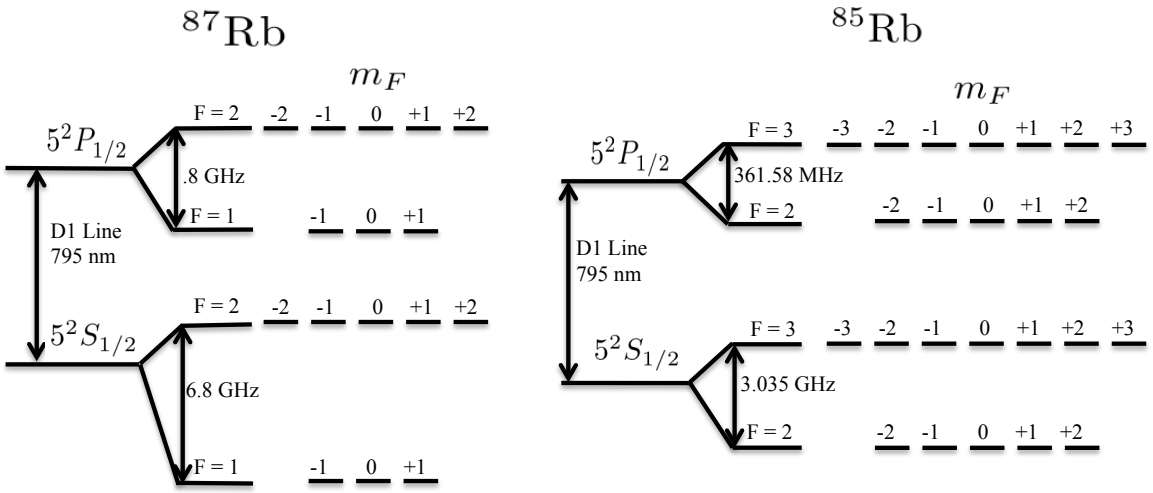

FIG. 1: The energy diagram for the D_1 line for ^{85}Rb and ^{87}Rb is shown along with the corresponding energy spacing. We find that in the presence of no external field, the hyperfine level F is degenerate. If a field is applied, then there is an energy spacing between m_F porportional to the strength of the field. The number of these levels correspond to 2F+1.

In this experiment we use frequencies in the kHz range to make transitions between m_F levels once the degeneracy is split. It is clear from the diagram above that we know transitions are made in the same hyperfine F level based on the large energy separation between F levels. We now have enough information to present the concept of optical pumping.

1.4. Optical Pumping

In this experiment the incident light on the Rb cell is σ^+ polarized. Due to the selection rules we find that no transition can occur unless $\Delta m = 0, \pm 1$ [6]. These solutions correspond to the three distinct polarization types which are π, σ^- and σ^+ with π referring to linear polarization, σ^- referring to left-hand circularly polarized and σ^+ referring to right-hand circularly polarized

light with respect to the direction of propagation. This experiment utilizes σ^+ polarized light to send atoms to the highest m_F level, which becomes a dark state, as it has nowhere to excite to after (since we block the D2 line). After a transition is made to an excited state, $m'_F = m_F + 1$, it will decay rapidly and spontaneously. It is important to recall that the lifetime is on the order of $\times 10^{-8} s$. When spontaneous decay occurs, the direction of emission is uniform in all directions and polarization of the emitted light is arbitary, in that it can make a transition of $\Delta m_F = 0, \pm 1$. This is indicated by the stripped line in the figure below.

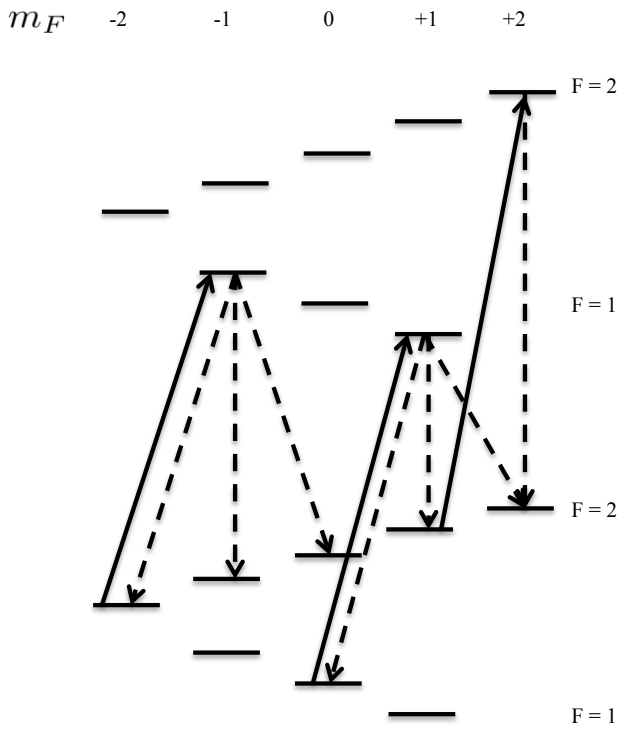

FIG. 2: Here the effects of σ^+ polarized light incident on an atom are shown. Since the light has angular momentum the selection rules tell us that for σ^+ light, $\Delta m = 1$ in a transition. We see this results in electrons going to the right. This diagram shows optical pumping to the F = 2, $m_F = +2$ level in ^{87}Rb. The same case is true in ^{85}Rb except we optically pump to F = 3, $m_F = +3$. Once the electron has undergone stimulated absorption, it will excite to a higher energy level. When it undergoes spontaneous emission the polarization of the light is random and therefore it can make any of the three transitions indicated by a dashed line. After many lifetimes of absorption and decay/emission we find all the electrons in the F = 2, $m_F = +2$ state. This is the dark state. In the case of σ^- light we can pump electrons to the left, to the F = 2, $m_F = -2$ in this case.

If the electron undergoes stimulated emission then the polarization it encounters will be σ^- sending it back to the original m_F level it started at. It quickly becomes clear that to effectively optically pump, the incident light on the atoms must be present over at least ten lifetimes. In our case, if we take the lifetime of the excited state to be 10^{-8} then in a full second we have $\approx 10^8$ cycles of absorption and decay or emission. Therefore, practically after only one second, the chances of all the electrons being optically pumped is very high. The efficiency is limited due to other factors that are noted in the Procedure section. At time t = 0 we assume that all the m_F states are equally populated due to thermal excitations, $k_bT \approx 10^{12}s >> GHz$. It must be noted that a static external field must be present to split the degeneracy of the m_f levels, otherwise we could not optically pump. Experimentally the magnetic field from the Earth, B_{earth}, is enough to split the degeneracy. Now let's look more in depth at how static fields perturbe the system.

1.5. Interaction with Static External Fields

This experiment utilizes a static magnetic field to split the degeneracy of the m_F levels. A similar phenomena occurs when there is a static electric field present but for the purposes of this experiment those such effects will not be discussed. As mentioned, each hyperfine level consists of 2F+1 degenerate sublevels, m_F. In the presence of an external magnetic field the degeneracy is broken.

$$H_B = \frac{\mu_B}{\hbar}(g_s S_z + g_L L_z + g_I I_z) \cdot B_z \tag{15}$$

Eq. (15) is the Hamiltonian[4][5] describing the interaction with the magnetic field along the atomic quantization axis. We see that the B field interacts with the magnetic dipole moments of the electron spin, electron orbit, and the nuclear spin. g_S, g_L, g_I are the electron spin, electron orbital, and nuclear "g-factors". Here, $g_L = 1 - m_e/m_{nucleus}$, which we approximate to 1. The exact value of g_s has been measured to high precision to be 2.00231930436153(53)[7] which we will approximate to 2 in this lab. To calculate g_J we look at the magnetic moment associated with J:

$$(\vec{\mu}_S)_J = [(\vec{\mu}_L)_J + (\vec{\mu}_S)_J] \cdot \frac{J}{|J|} \tag{16}$$

where

$$(\vec{\mu}_L)_J = \frac{\mu_B}{2}\frac{\vec{L}\cdot\vec{J}}{|J|} \qquad (\vec{\mu}_S)_J = -2\frac{\mu_B}{2}\frac{\vec{S}\cdot\vec{J}}{|J|} \ . \tag{17}$$

Solving for $\vec{\mu}_J$ we find,

$$\vec{\mu}_J = -\frac{\mu_B}{2}\left[\frac{3}{2} + \frac{S(S+1) - L(L+1)}{J(J+1)}\right]\vec{J} \ , \tag{18}$$

which gives us[3],

$$g_J \simeq \frac{3}{2} + \frac{S(S+1) - L(L+1)}{J(J+1)} \ . \tag{19}$$

The g-factor to consider is g_F. Again we look at the magnetic moment associated with $\vec{F}$. Solving in the same fashion as above we find,

$$\vec{\mu}_F = -g_J\frac{F(F+1) + J(J+1) - I(I+1)}{2F(F+1)}\frac{\mu_B}{\hbar}\vec{F} \ , \tag{20}$$

which gives us a value of g_F where we neglect the nuclear term because it is a correction of .1%. We repeat this approximation below for the final form the Hamiltonian for the same reason.[3][4][5]

$$g_F \simeq g_j\left[1 + \frac{J(J+1) - I(I+1)}{F(F+1)}\right] \ . \tag{21}$$

Writing the Hamiltonian for the hyperfine structure's interaction with an external magnetic field we find[3],

$$H_{HFS} = A(\vec{I}\cdot\vec{J}) - \vec{\mu}_J\cdot\vec{B}_0 - \vec{\mu}_I\cdot\vec{B}_0 \simeq A(\vec{I}\cdot\vec{J}) - \vec{\mu}_J\cdot\vec{B}_0 \ , \tag{22}$$

where $A(\vec{I}\cdot\vec{J})$ is the term describing the internal state and $-\vec{\mu}_J\cdot\vec{B}_0$ describes the interaction with the external field. A is the magnetic dipole constant [Hz], dependent on the fine structure state, and has values given in References [4][5].

1.5.1. Zeeman Effect

In the weak field limit where J is a good quantum number, $|-\vec{\mu}_J\cdot\vec{B}_0| \ll |A(\vec{I}\cdot\vec{J})|$. We see that $\vec{F}$ precesses around $\vec{B}_0$. In this limit, the external field acts as a perturbation on the hyperfine structure. Thus the energy term can be solved to find,

$$\Delta E_{|Fm_F>} = h\nu = \mu_B g_F m_F B_z \ , \tag{23}$$

where $h = 6.62606957(29) \times 10^{-34} Js$ = Plancks constant, $\mu_B = 9.27400968(20) \times 10^{-24} JT^{-1}$ = Bohr Magneton, B_z is the magnetic field in the axis of quantization, m_F = change in sublevel number and g_F is the *Landé* g-factor for the hyperfine level. This equation describes the energy separation between magnetic sublevels m_F, for a given hyperfine structure F in the weak-field limit. This regime of splitting is called the *Zeeman effect*. We see that if we use the theoretical values for g_F given by Equation (21) one can solve for the external B field.

$$B_z = \frac{\Delta E}{\mu_B g_F m_F} = \frac{h\nu}{\mu_B g_F m_F} \tag{24}$$

We use this to solve for the Earth's magnetic field, B_{earth} by finding the center frequency, ν and using a theoretical value for g_F, where $m_F = 1$.

When we rearrange the terms, we find

$$g_F = \frac{h\nu}{\mu_B m_F B_z} \ . \tag{25}$$

This equation can be used to give precise measurements of g_F by plotting the absorption frequency ν, which corresponds to ΔE, versus the applied magnetic field, B_z. The slope of the resulting line is porportional to g_F. This is the procedure we used to measure the grand angular momentum g-factor, g_F.

1.5.2. Strong Fields

Considering the strong field limit where $|-\vec{\mu}_J \cdot \vec{B}_0| \gg |A(\vec{I} \cdot \vec{J})|$ we find that the interaction term dominates the hyperfine energies, and thus the hyperfine Hamiltonian is a perturbation on the strong-field eigenstates $|J\, m_J\, I\, m_I\rangle$[4][5].

$$\Delta E = g_j m_j \mu_B B_0 + A m_I m_J \tag{26}$$

This expression gives the energy separation in the strong field regime, between m_I states for a given m_J value, where $Am_I m_J$ is a small correction that arises since $\vec{I}$ and $\vec{J}$ both precess around $\vec{B}_0$ due to the I-J coupling[3]. The energy shift in this regime is called the *Paschen-Back effect*.

Dealing with the intermediate case requires one to diagonalizable $H_{HFS} + H_B$ which becomes more difficult to compute. In this experiment we do not take measurements in this regime but discussions regarding it can be found in References [3],[4] and [5].

1.6. Spin Resonance

Classically we know that a magnetic moment will precess around a static magnetic field at the Lamour frequency, $w_L = \gamma B_0$. Changing our reference frame into the rotating frame of the magnetic moment we find

$$\frac{d\vec{J}}{dt} = \gamma \vec{J} \times \left(\vec{B}_0 + \frac{\omega}{\gamma} \right) = \vec{B}_{0,eff} \ , \tag{27}$$

which we discover to be zero if $\vec{\omega} = -\gamma \vec{B}_0$. The gyromagnetic ratio, $\gamma = g\mu_B/\hbar$ in the quantum mechanical treatment. Now lets add an additional rotating magnetic field $\vec{B}_1 = B_1(cos(\omega t)\vec{e}_x - sin(\omega t)\vec{e}_y)$ which is analogous to the RF signal in this experiment. If $\omega = \omega_L$ the magnetic moment only experiences $\vec{B}_1(t)$ and thus precesses around $\vec{B}_1(t)$, which is static in rotating frame, with $\omega_R = \gamma B_1$ which is our Rabi frequency.

If $\omega \neq \omega_L$ then,

$$\vec{B}_{eff} = \vec{B}_1 \vec{e}_{rot} + \left(\vec{B}_0 - \omega/\gamma \right) \vec{e}_z \qquad |\vec{B}_{eff}| = \sqrt{B_1^2 + \left(\vec{B}_0 - \omega/\gamma \right)^2} \ . \tag{28}$$

We find the two terms precess around $\vec{B}_{eff}$ at a rate,

$$\Omega_R = \gamma B_{eff} = \sqrt{\omega_R^2 + (\omega_L - \omega)^2} = \sqrt{\omega_R^2 + \delta^2} \ . \tag{29}$$

In the analogy of a two-state system, if $\omega = \omega_L$ it is possible to achieve full inversion. If $\omega \neq \omega_L$ then we have a case where the state may not invert. Further investigation shows we can use principles describing the time evolution of a two-state system to completely describe how the RF signal excites transitions between m_F sublevels.

We already know the interaction term is written $H = -\vec{\tilde{\mu}} \cdot \vec{B}$. Here $\vec{\tilde{\mu}}$ is written as follows:

$$\vec{\tilde{\mu}} = \frac{\gamma \hbar}{2} \vec{\tilde{\sigma}} \tag{30}$$

with

$$\vec{\hat{\sigma}} = (\hat{\sigma}_x, \hat{\sigma}_y, \hat{\sigma}_z) \tag{31}$$

are just Pauli's matrices. Plugging this in to H we find,

$$H = -\frac{\hbar}{2}\gamma B_0 \hat{\sigma}_z - \frac{\hbar}{2}\gamma B_1 (cos(\omega t)\hat{\sigma}_x + sin(\omega t)\hat{\sigma}_y) = -\frac{\hbar}{2}\omega_L \hat{\sigma}_z - \frac{\hbar}{2}\omega_1 (cos(\omega t)\hat{\sigma}_x + sin(\omega t)\hat{\sigma}_y) \tag{32}$$

Plugging in for $\hat{\sigma}_x, \hat{\sigma}_y, \hat{\sigma}_z$ we find,

$$i\hbar \begin{pmatrix} \dot{\tilde{a}}_g \\ \dot{\tilde{a}}_e \end{pmatrix} = -\frac{\hbar}{2} \begin{pmatrix} \omega_L & \omega_1 e^{-i\omega t} \\ \omega_1 e^{i\omega t} & \omega_L \end{pmatrix} \cdot \begin{pmatrix} \tilde{a}_g \\ \tilde{a}_e \end{pmatrix} \tag{33}$$

,

which is the time evolution of a two-state system under a time dependent perturbation found from the Shroëdinger equation[3][6][8]. Imparting the rotating-wave transformation with rotation operator $\hat{D}_z(\phi) = e^{-i\hat{S}_z\phi/\hbar}$ on ψ we get,

$$|\psi\rangle = \tilde{a}_g e^{-i\phi/2} |g\rangle + \tilde{a}_e e^{-i\phi/2} |e\rangle = c_g |g\rangle + c_e |e\rangle \tag{34}$$

where $\phi = \omega t$. Making the substitution $\delta = \omega - \omega_L$ we find,

$$i\hbar \begin{pmatrix} \dot{\tilde{c}}_g \\ \dot{\tilde{c}}_e \end{pmatrix} = -\frac{\hbar}{2} \begin{pmatrix} -\delta & \omega_1 \\ \omega_1 & \delta \end{pmatrix} \cdot \begin{pmatrix} \tilde{c}_g \\ \tilde{c}_e \end{pmatrix} \tag{35}$$

.

This coupled differential equation is analogous to an optically driven 2-level atom. Recall we have a well defined Rabi frequency $\omega_R = \gamma B_1$ with a detuning $\delta = \omega - \gamma B_0$. The two coefficients describe the time evolution of the system as it falls to the ground state $c_g = 1, c_e = 0$ at time $t = \pi/\omega_R$ and is excited back to $c_e = 1, c_g = 0$ at time $t = 2\pi/\omega_R$. By imparting the following initial conditions we find that the solution to this differential equation is as follows:

$$\begin{pmatrix} c_g(0) \\ c_e(0) \end{pmatrix} = \begin{pmatrix} 0 \\ 1 \end{pmatrix} \tag{36}$$

These are chosen because of experimental reasons. We start at the highest m_F sublevel and can only excite down to the "ground state" which is just the next lower m_F level. Thus,

$$\begin{pmatrix} \tilde{c_g} \\ \tilde{c_e} \end{pmatrix} = \begin{pmatrix} cos(\frac{1}{2}\Omega_R t) - i\frac{\delta}{\Omega_R} sin(\frac{1}{2}\Omega_R t) \\ i\frac{\omega_R}{\Omega_R} sin(\frac{1}{2}\Omega_R t) \end{pmatrix}, \Omega_R \equiv \sqrt{\omega_R^2 + \delta^2} \ . \tag{37}$$

It is more convienent to write the states as a function of their probability density, P_g or P_e which are defined below.

$$P_g = \tilde{a}_g \ \tilde{a}_g^* = c_g c_g^* = 1 - P_e \tag{38}$$

$$P_e = c_e c_e^* = \frac{{\omega_R}^2}{\Omega_R} sin^2(\frac{1}{2}\Omega_R t) \ . \tag{39}$$

Here, we see if $P_g = 1$ then $P_e = 0$ and the system is in the ground state and the same goes with $P_e = 1$, the system is in the excited state. We can also tell from this formula that if $\delta = \omega - \omega_L = 0$ then $\omega_R/\Omega_R = 1$ resulting in a maximum amplitude of 1 (probability cannot be greater than 1). Otherwise if $\delta \neq 0$ our amplitude is reduced, so is the probability of the state making a transition. Additionally, if $\Omega_R = \omega_R$ the frequency of oscillation is minimized unless $\Omega_R > \omega_R$ which leads to a higher frequency.

1.7. Power and Doppler Broadening

It is important to note certain aspects of the experiment that can affect the lineshape of the absorption dip. One key factor is Doppler Broadening which describes the change in frequency that an atom traveling with velocity v may encounter. Doppler Broadening causes the absorption dip to take a Gaussian functional form instead of the natural Lorenztian. This is shown below

$$\omega^{'} = \omega \pm kv \ , \tag{40}$$

where ω is the angular frequency of the radiation, $k = \frac{2\pi}{\lambda}$ is the wavenumber of the radiation, and v is the velocity of the atom. We choose to add the terms for the atom traveling towards the direction of propagation of the radiation, and a minus sign for the atom traveling away from the direction of propagation. If one solves for $\omega^{'}$ using $f = 200kHz$ and $v = 100m/s$, one finds that the change in frequency observed is $\simeq mHz$. This should hardly produce any effects on the absorption lineshape, which is naturally Lorentzian. Some of the preliminary data has shown

Gaussian functions to fit better than a Lorentzian but we believe that is due to some other effects. Since we are primarily concerned with the center frequency, and not the overal lineshape, our goal is to use a fitting function resulting in the most accurate determination of this value. Regardless the broadening of the lineshape needs to be addressed.

The other effect that can vary the absorption lineshape is power broadening. When the radiation power hits a saturation point with respect to a two-level system going through stimulated absorption/emission then the absorption dips haven been shown to broaden[4]. Although the affect of power broadening will not change the functional form of the lineshape, it will broaden the edges of the absorption dip. We study the effects of changing amplitudes and present our information in Section 3.1.

2. PROCEDURE

2.1. Apparatus

In the experimental setup a Harrison Lab DC Supply feeds 16V to a Rb Lamp, which emits light over a range of frequencies but consists of predominately the D_1 line $\lambda_1 = 794.76$ nm and the D_2 line $\lambda_2 = 780.02$ nm. The light is focused by a lens and then passes through an interference filter (based off the principles of a Fabry-Perot) which blocks out the D_2 line light. This light also passes through a linear polarizer followed by a quarter-wave plate to circularly polarize the D_1 light. The light is now σ^+ or right hand circularly polarized. The selection rules tell us that for σ^+ polarized light the only stimulated transitions between states that can be made are for $\Delta m = +1$.[6]

The light passes through a Rb vapor cell (which is heated to about $50°C$) and excites electrons from the first electronic ground state of Rubidium $5s^2S_{1/2}$ to $5p^2P_{1/2}$ via the D_1 line. After many lifetimes of absorption and emission (spontaneous or stimulated) the electrons are pumped to the highest m_F level of the $5s^2S_{1/2}$ state; in ^{85}Rb F = 3 $m_F = +3$ and in ^{87}Rb F = 2 $m_F = +2$. This is due to reasons explained in Section 1.4. Because we have blocked the D_2 line, the electrons are now in a dark state, meaning they cannot excite to a higher energy state. That is, based upon the polarization of the light, σ^+, there is no $m_F = +3$ state to excite to for ^{87}Rb and no $m_F = +4$ state to excite to in ^{85}Rb since we have blocked the D_2 line. If it were present then excitation would occur because these sublevels exist in the $5p^2P_{1/2}$ state.

It should be noted that not 100% of the electrons are optically pumped. Various relaxation

processes including collisions with the walls of the cell and collisions with other atoms, cause deexcitation. In our cell, an Argon buffer gas acts to prevent most atoms from hitting the wall but instead Rb atoms collide with the Argon atoms. The cost of having the Argon gas present is that when a collision occurs, the energy levels of Rb are smeared out, or pressure broadened. This is accounted for by heating the Rb Cell to an optimum temperature where the resonant dips are not widened due to this effect.[2]

The light that passes through the Rb cell is focused onto a Silicon photodiode, powered by a 9V battery, which outputs a voltage to an Agilent 34401A Digitial Multimeter. The reading on the multimeter is fed to a computer and read using LabVIEW. To efficiently optically pump, it is necessary to excite the state a number of lifetimes, in the order of ten, for the electrons to be pumped to the desired states. This means that in approximately .2 ns the electrons are optically pumped to a dark state at which time no absorption of the light occurs and the photodiode reads a steady voltage. Measurements in this experiment are attributed by applying an RF signal through Helmholtz coils that surrond the Rb cell, perpindicular to the Maxwell coils. The reason for this is based upon the principles of Section 1.6 where the field produced by the Maxwell coils is denoted by B_0 and the field from the Helmholtz coils is B_1. The Helmholtz coils consist of two loops of an unknown number of turns of 0.0812(5) cm diameter copper wire.[2] The coils are of radius r, separated by their radius (center to center) as required in a Helmholtz coil configuration. A HP 3330B Synthesizer is used to generate RF frequencies in the kHz range. The RF radiation is used for stimulated emission to drive the electron to the next lower m_F level in the hyperfine structure; F = 2 $m_F = +1$ for ^{87}Rb and F = 3 $m_F = +2$ for ^{85}Rb. In this new state, the electrons can now excite to the $5p^2P_{1/2}$ state via the D_1 line. Due to the short lifetime, the electrons fall back to either m_F level and the process repeats only if the transition is fully saturated. This means that the cycle repeats roughly 10^9 times in a second. As a result enough energy is absorbed by the atoms, from the light field, to be detected by the photodiode. As a means of detecting resonance, as we start the frequency sweep a certain range of frequencies will drive this transition and thus absorb energy which will show as an absorption dip read by the photodiode. As discussed, Section 1.7, this lineshape is affected by various process'.

The RF synthesizer has two outputs. One is input to a PRD Model 7805 Amplifier and the other output is connected to an Agilent 34401A Digital Multimeter. The PRD Amplifier sends an output signal to the Helmholtz coils which drives the transitions between magnetic sublevels. In Section 3.1, we study the gain from the amplifier as a function of input frequency. The Agilent Digital Multimeter is connected to a computer which also is read on LabVIEW in terms of a

voltage sweep. If one records the center frequency, step size, and number of steps in the frequency sweep it is possible to scale the voltage sweep to a frequency sweep since the relationship is linear. Recording the frequency sweep in LabVIEW and the voltage read by the photodiode one has all the necessary components to observe resonance corresponding to absorption dips.

Figure 3 shows a diagram of the experimental set up. We now have enough information to understand the data collection process. Now lets look into Maxwell Coils.

2.2. Maxwell Coils

This experiment utilizes a Maxwell coil configuration to produce a homogeneous magnetic field through its center. The field produced is more uniform than that produced by Helmholtz coils. Fig. 3 shows the relationships between the center coil's radius R and the number of turns N to the radius of the outside coils, the distance from the center coil, and the number of turns. We find that if a current runs through the wires in the coils a magnetic field is produced which runs through the center of each coil. The direction of the magnetic field lines are parallel or antiparallel to the propagation of the D_1 line light depending on the direction the current runs through the wires as described by the right hand rule. As stated the Maxwell coil produces a uniform field through its center which is essential so that each Rb atom 'see' the same magnetic field otherwise the inaccuracy in our measurements would be large, recall Avagadros number. The coils are wound with 0.132(5) cm diameter copper wire. In the center coil 'B' there are 14 layers of wire, with 11 turns in odd-numbered layers and 10 turns in even numbered layers with the exception of layer 14 which has 5 turns making a total of 142 turns. The diameter of coil 'B' is 78.4(5) which is measured to the innermost layer. At a distance of 26.2(2) cm in both directions (from center to center) are coils 'A' and 'C'. Each coil has 11 turns in odd numbered layers and 10 turns in even numbered layers again with the exception of the outermost layer, 11, which has 5 turns. Each small coil has an inner diameter of 59.1(5) cm.[2]. In Section 3.3 we use the Biot-Savart Law to determine the magnetic field produced by the Maxwell coil as a function of current through the wires. The current is supplied by a HP 6011A DC Power Supply. We measure the current in series using a Keithley 199 Trims Digital Multimeter.

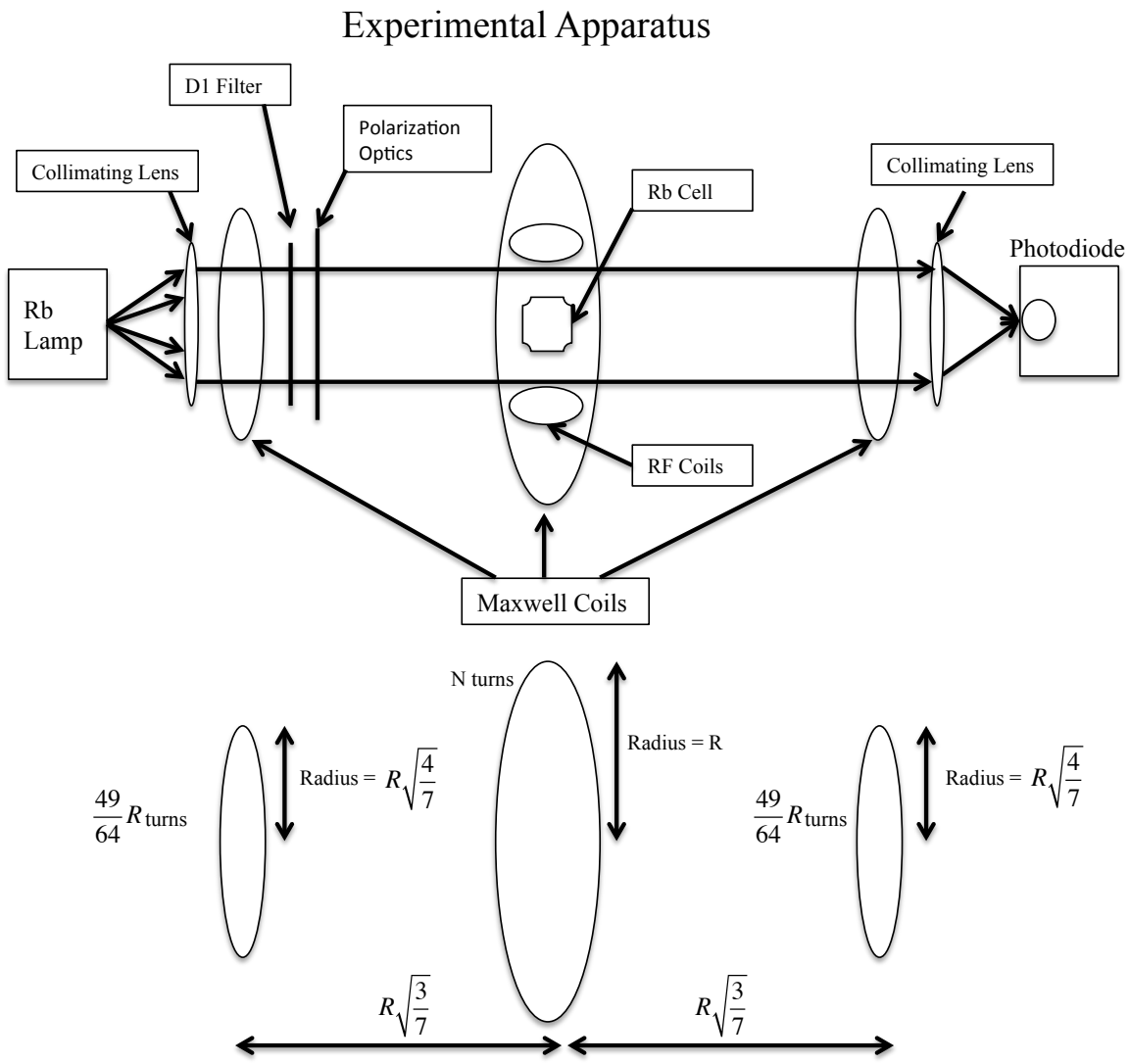

FIG. 3: This is a diagram of the experimental apparatus, which is approximately .745m (long not including the base). It is set at an angle of approximately 30° to the floor. A Rb lamp emits a range of wavelengths consisting of primarly the D_1 and D_2 line. It passes through a collimator, D_1 filter to block the D_2 light, a linear polarizer and a quarter-wave plate all of which generates circularly polarized light. The light is incident on the Rb cell and the transmitted light is read onto a photodiode. When absorption occurs the transmitted power decreases which is detected by the photodiode. The setup for the Maxwell Coils are shown including their dimensions. The RF coils which provide the kHz frequency to make transitions between m-sublevels are in a Helmholtz coil configuration which means they are seperated by their radius with an equal amount of turns.

3. DATA AND ANALYSIS

Once resonance has been observed, the experiment allows plenty of room to measure various phenomena. We first measured the effects of power broadening in the ^{87}Rb isotope. We used this to determine an optimum amplitude range providing us with a clean absorption dip making the fitting more precise. Afterward we measurd B_{earth} by determining the center frequency of a transition and by using theoretical values of g_F in each isotope from references [4],[5]. Once these values are known we can then calculate B_{earth} from Eq. (24). Afterward we apply a current through the Maxwell coils to produce a magnetic field to change the energy separation between magnetic sublevels in a controlled manner. These effects are studied in the weak and strong field regimes. In both these cases, and as seen with the Earth's magnetic field calculation, we use GNUplot to fit a Gaussian function, utilizing the method of least squares fit to determine the center frequency of the absorption dip. The fitting function has the form:

$$f(x) = ae^{-\frac{(x-b)^2}{2c^2}} + d \ . \tag{41}$$

Naturally the lineshape should have a Lorentzian form, but various experimental effects produce an absorption dip that takes a Gaussian form. Our measurements are concerned with the value of the center frequency which is why we chose to use a Gaussian fitting function.

3.1. Power Broadening

As discussed, one factor contributing to a widened lineshape is power broadening. Here we measure the lineshapes in ^{87}Rb for various output amplitudes from the HP 3330B Synthesizer. Recall the output signal from the synthesizer is connected to a PRD Model 7805 (RF) Amplifier. The first thing we did was to measure the frequency dependence on the amplified signal for a fixed amplitude on the synthesizer. Due to the nature of sweeping the frequency, it is important to determine this relation. We find that the amplified signal responds differently for various input frequencies. This is probably due to the internal circuitry of the RF amplifier.

From the figure we verify that the RF amplifiers gain is dependent on input frequency. We are are also able to determine a saturation point, where the RF output reads overdrive, in which the gain is too high for the amplifier. It also provides reason behind why we have to change the synthesizer amplitude to -10dBm when measuring the energy separation in the strong field regime.

This is due to the fact that there is no gain from the amplifier for -35dBm input at high frequencies, shown below.

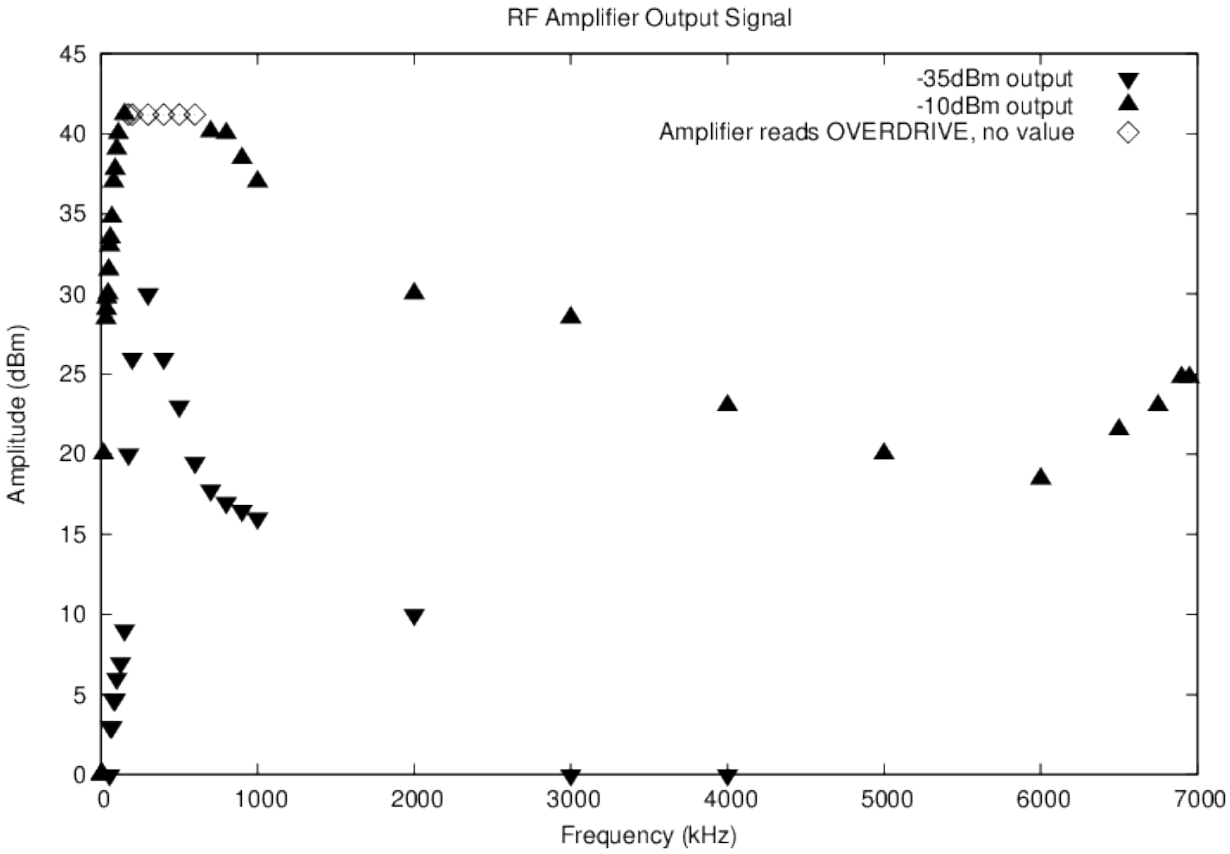

FIG. 4: Here a HP 3330B Synthesizer's output signal is input to a PRD Model 7805 Amplifier. We find the amplification from the PRD is dependent on the input frequency. Here two different amplitudes are set on the synthesizer while the frequency is stepped. While the PRD notes a 47dBm gain we find a saturation point around 41dBm.

The next step was to sweep over a range of amplitudes on the synthesizer. The goal was to obtain an optimum ratio between signal strength and broadness of the lineshape. We also wanted to resolve apparent asymmetries in the lineshape. In this case we used the ^{86}Rb isotope as our test signal. The frequency sweep was centered at 304.75 kHz with a 1000 steps of 10 Hz at 30ms/step. Below is a plot showing the various lineshapes for different amplitudes set by the sythesizer.

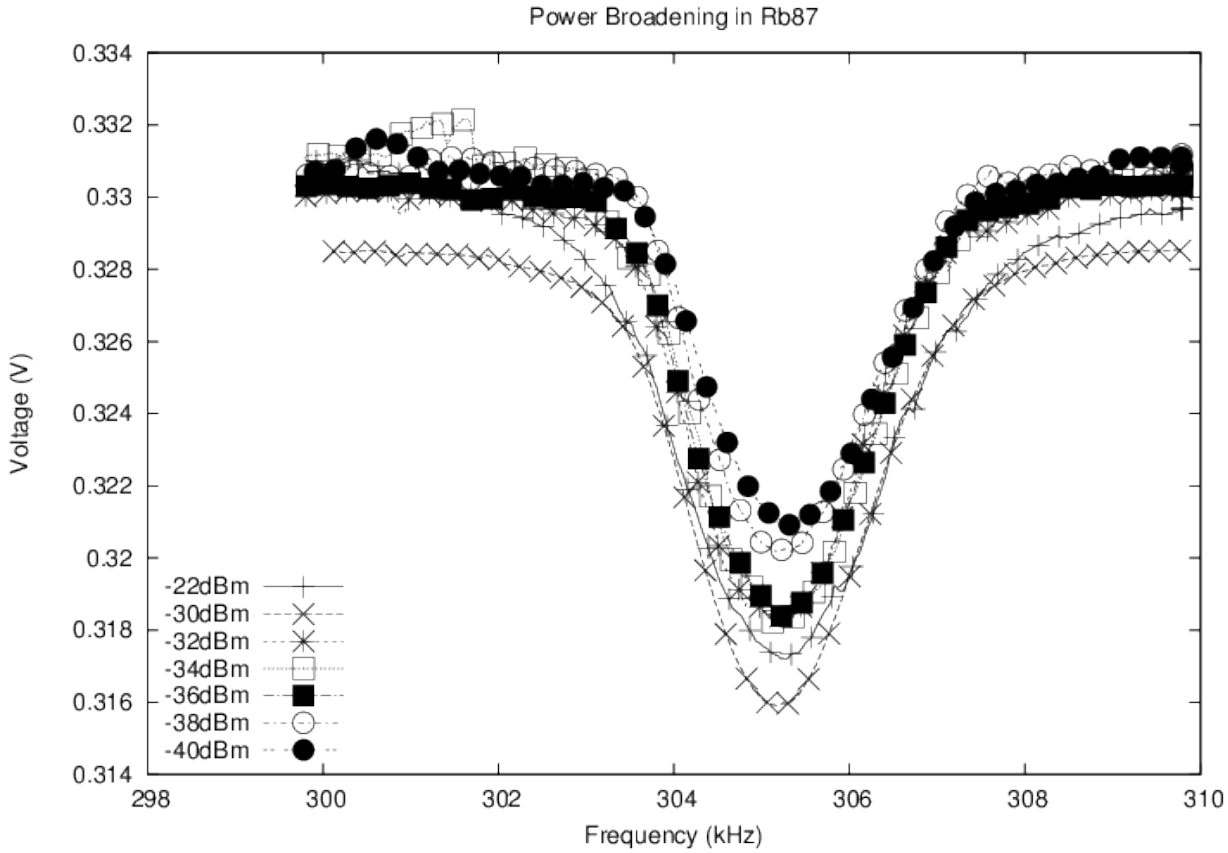

FIG. 5: The absorption dip for ^{87}Rb is shown here for various amplitudes set on the frequency synthesizer. We see that the wave shape goes from having a slight asymmetry to symmetric with decreasing amplitude. This graph is also a good indicator of one form of error we have in our data collection methods which is a DC drift of the baseline voltage. Based on the results of the graph, we found that a optimum value for the amplitude set by the synthesizer is between -36dBm and -40dBm. Note that in the strong magnetic field regime, when the RF frequency is high, we need to use a higher power to resolve the absorption which we choose to be -10dBm. This is explained by Fig.5 which shows the frequency dependence of the RF amplifier.

Based upon these results we find that the optimum range of amplitude, before passing through the amplifier, which is -47dBm to -32dBm. The asymmetries are corrected in the applied field as the amplitude is lowered. As an aside, other reasons for the asymmetries in the lineshape are due to pressure broadening from collisions of atoms in the Rb Cell. As stated, a buffer gas of Argon is added to reduce this effect but it is still present. This is our motivation for choosing our primary amplitude to be -35 dBm. We did not choose -40dBm, as this graph would indicate, because of the frequency dependence on the RF amplifier. At -35dBm, the range at which we could resolve dips in terms of frequency was larger than -40dBm. We see in later sections that we have to increase

the amplitude to resolve the dips of each transition at higher input frequencies.

3.2. Measuring the Earth's B Field

When there is no current in the Maxwell Coils, the presence of the Earth's magnetic field is enough to break the degeneracy of the hyperfine structure. We have shown that in this regime, *Zeeman effect*, it is possible to find use theoretical values for g_F to find B_{earth}. There is also the presence of ambient magnetic fields from other experiments in this laboratory but we neglect them because they are much smaller than the magnitude of the Earths field. Here we use Eq. (24) to determine the B field, using theoretical values for g_F: for ^{85}Rb F=3 $g_F = 1/2$ [2] and for ^{87}Rb F=2 $g_F = 1/3$ [3].

Changes in this value may vary because: the field itself is moving, alignment with the apparatus, and ambient magnetic fields present in the laboratory. All these factors contribute to the variability in B_{earth}.

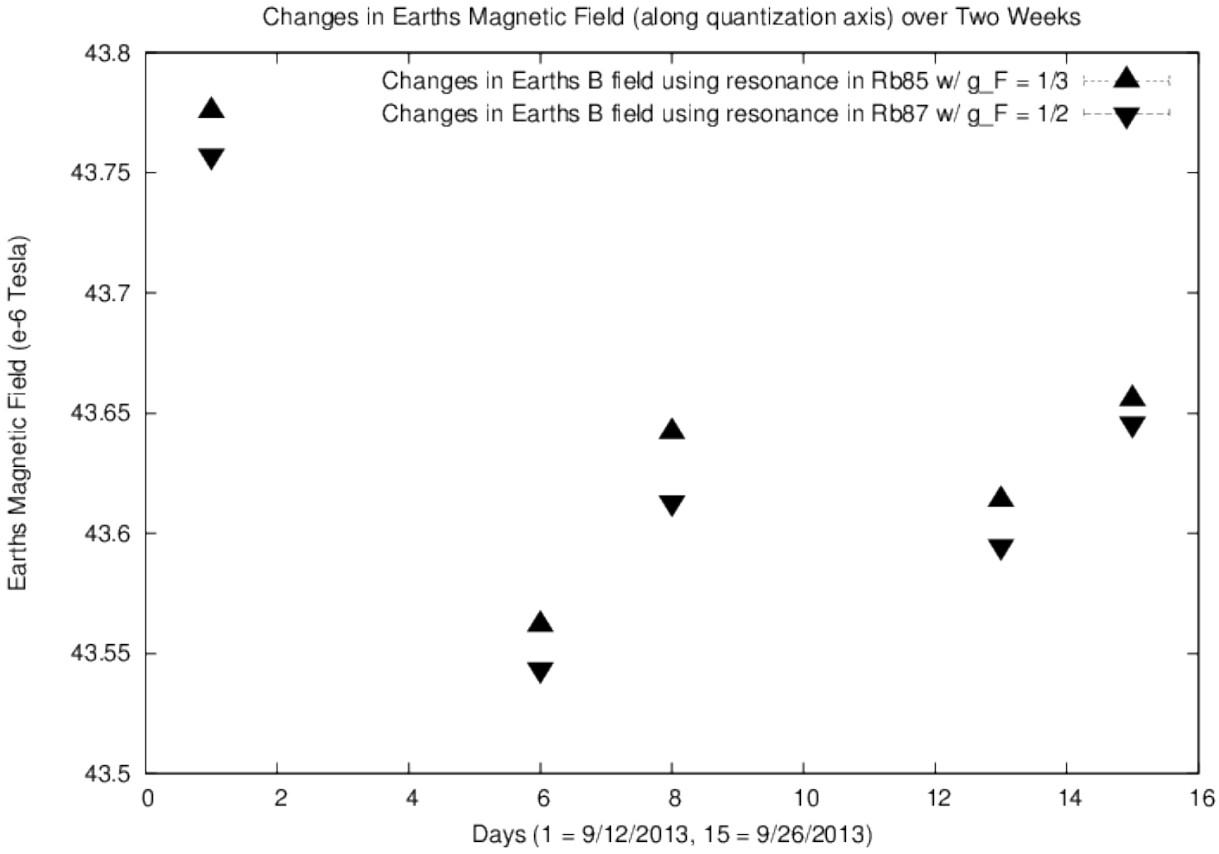

FIG. 6: The Earth's magnetic field strength along the quantization axis, z, is shown here. We used the absorption frequencies in both isotopes to give comparable measurements over a period of two weeks.

If we take the average of the B field found from the ^{85}Rb absorption resonance we find $B_{earth}(avg) = 43.6498(50)\mu T$ and for the ^{87}Rb isotope we find that $B_{earth}(avg) = 43.6309(37)\mu T$. While these values are not within error range of each other, they only differ by .04% giving us reason to trust these calculations. This also implies that we are correctly identifying which absorption dip corresponds to which isotope. Otherwise the calculated values would be incorrect by an amount proportional to the corresponding g-factor. Once we have measured this value, we can split the separation between m_F levels even further by applying an external field. In doing so, we also find an external field strength such that it cancels the Earth's magnetic field which is indicated by observing no absorption dips over a frequency sweep. This is because there is no breaking of the degeneracy in the m_F levels and also gives us another measurement of the Earths field to compare to the calculations done here.

3.3. The Magnetic Field Produced By Maxwell Coils

The magnetic field produced by a loop of N turns, radius r, and current I is described by the Biot-Savart Law.

$$\vec{B} = \frac{N\mu_0 I}{4\pi} \oint_C \frac{d\vec{l} \times \vec{r}}{|\vec{r}|^3} \tag{42}$$

Solving this equation for the magnetic field at a distance z above the center of the coil we find,

$$\vec{B} = \frac{N\mu_0 I}{2} \cdot \frac{r^2}{(\mathscr{z})^{3/2}}, \mathscr{z} = r^2 + z^2 \tag{43}$$

Using propagation of error we find that $\Delta\vec{B}$ is,

$$\Delta\vec{B} = \vec{B}\left(\frac{\Delta I}{I} + 2\frac{\Delta r}{r} + 3\frac{\Delta \mathscr{z}}{\mathscr{z}}\right) \tag{44}$$

The full expression of $\vec{B}$ is

$$\vec{B} + \Delta\vec{B} = \frac{N\mu_0 I}{2} \cdot \frac{r^2}{(\mathscr{z})^{3/2}}\left(1 \pm \left(\frac{\Delta I}{I} + 2\frac{\Delta r}{r} + 3\frac{\Delta \mathscr{z}}{\mathscr{z}}\right)\right. \tag{45}$$

We used a Matlab script to sum the individual contribution each layer in each coil has to the magnetic field at the Rb cell which is at the center of coil 'B' as a function of the applied current.

We also considered the error in these calculations. The error increases as B increases because we are multiplying a constant percent error by an increasing B field. The results of our calculations are shown below.

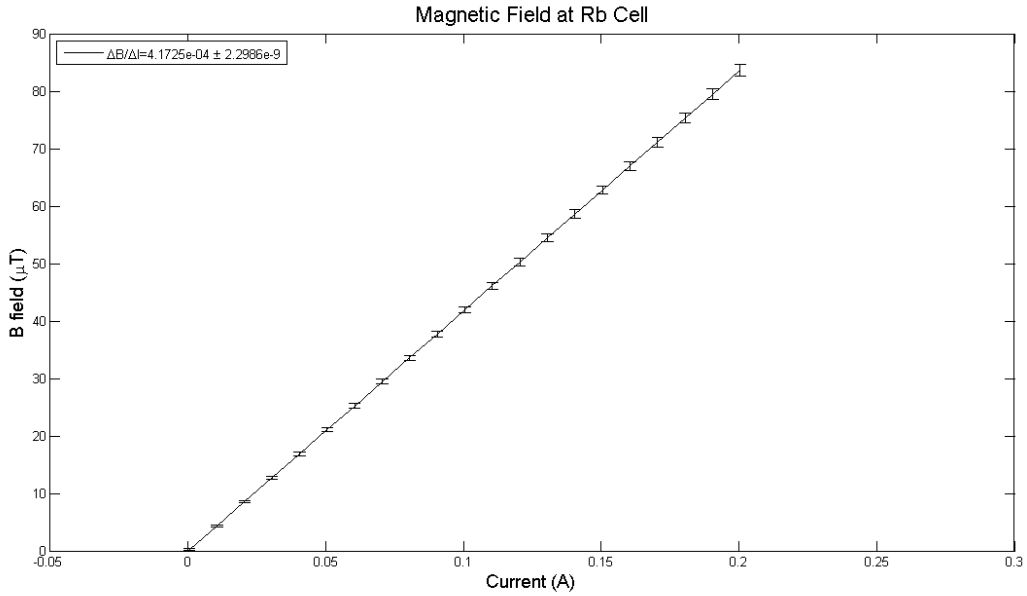

FIG. 7: Using a Matlab script, we were able to determine the magnetic field at the center of a Maxwell coil as a function of the current. By determining the slope of the line (T / A) we can then relate what the magnetic field is for a given current.

We see from the graph that the slope is $\Delta B/\Delta I = 4.1725 \times 10^{-05} \pm 2.2986 \times 10^{-9}$ [T/A] . This allows us to calculate the magnetic field **B** for any given current **I** by multiplying the slope by a given current. We use this to scale a given current to its corresponding magnetic field accordingly in the following sections.

3.4. Weak Field Measurements

Continuing the concepts from the above sections we know that when an applied magnetic field is small, such that it acts on a perturbation to the hyperfine structure, the energy separation between magnetic sublevels in the hyperfine structure is given by,

$$\Delta E_{|Fm_F>} = h\nu = \mu_B g_F m_F B_z \tag{46}$$

Thus as we vary the current through the coils, **I**, we also vary **B** linearly as described in the previous section. By sweeping through a range of current we are able to observe what the new value of ΔE by measuring the center frequency of the absorption dip. Below is an example showing the absorption dip and the corresponding fitting function for a given current in the Maxwell Coils.

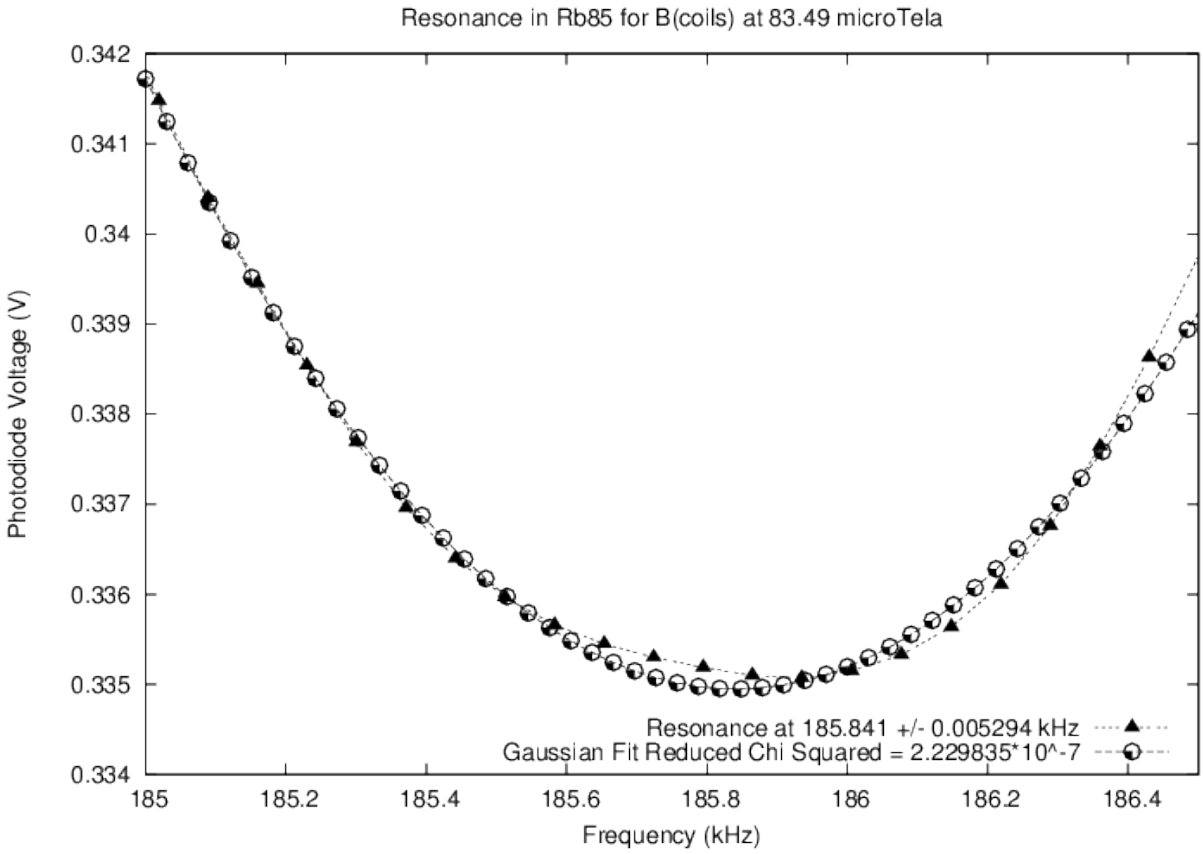

FIG. 8: A 185.841 ± 0.005294 kHz separation between $m_F = +3 \rightarrow +2$ absorption dip for $^{85}Rb$is shown here. A current of 200.1 mA in the Maxwell coil produces an external field of magnitude 83.4915(22) μT (not subtracting the Earths field). One must include the Earths field to give the total B field, which causes this given frequency gap, the atoms see in the Rb cell. We see that the center frequency is slightly asymmetric which is the reason why we zoom in on the center frequency. In doing so we can measure our center frequency with good precision.

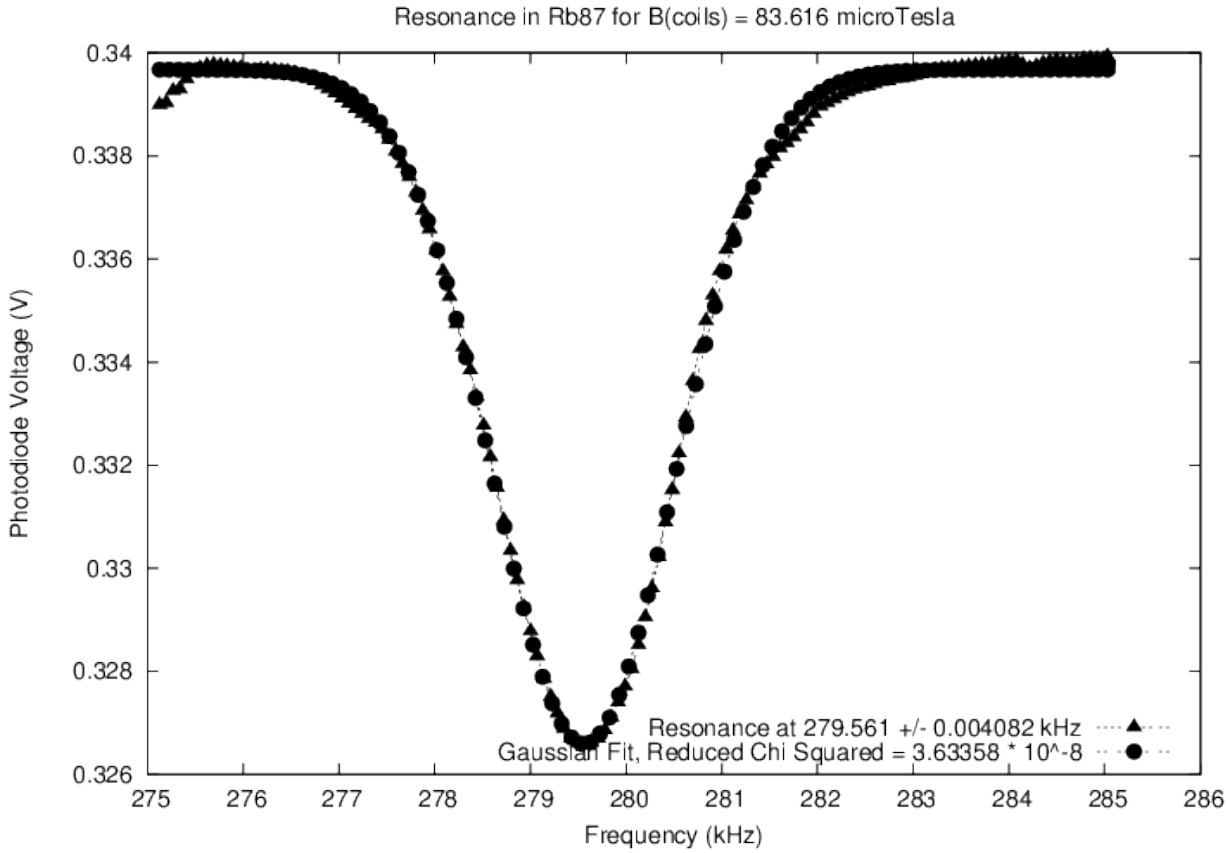

FIG. 9: A 279.561 ± 0.004082 kHz separation between $m_F = +2 \rightarrow +1$ absorption dip for ^{87}Rb is shown here. A current of 200.4 mA in the Maxwell coil produces an external field of magnitude 83.6169(22) μT (not subtracting the Earths field). One must include the Earths field to give the total B field, which causes this given frequency gap that the atoms see in the Rb cell. This graph showcases the accuracy of the fitting which is reflected in the reduced χ^2 value.

The figures below showcases that the signal observed when the applied B field through the coils is equal and opposite the magnitude of the Earth's field. We were able to do this by making the polarity of the current running through the Maxwell coil such that it produced a magnetic field in the direction (directed floor to ceiling) opposite that of the Earth's field (coming from the ceiling towards the floor). In doing so there is no splitting of the degeneracy of the magnetic sublevels in the hyperfine structure which means no transitions can be made between m_F states.

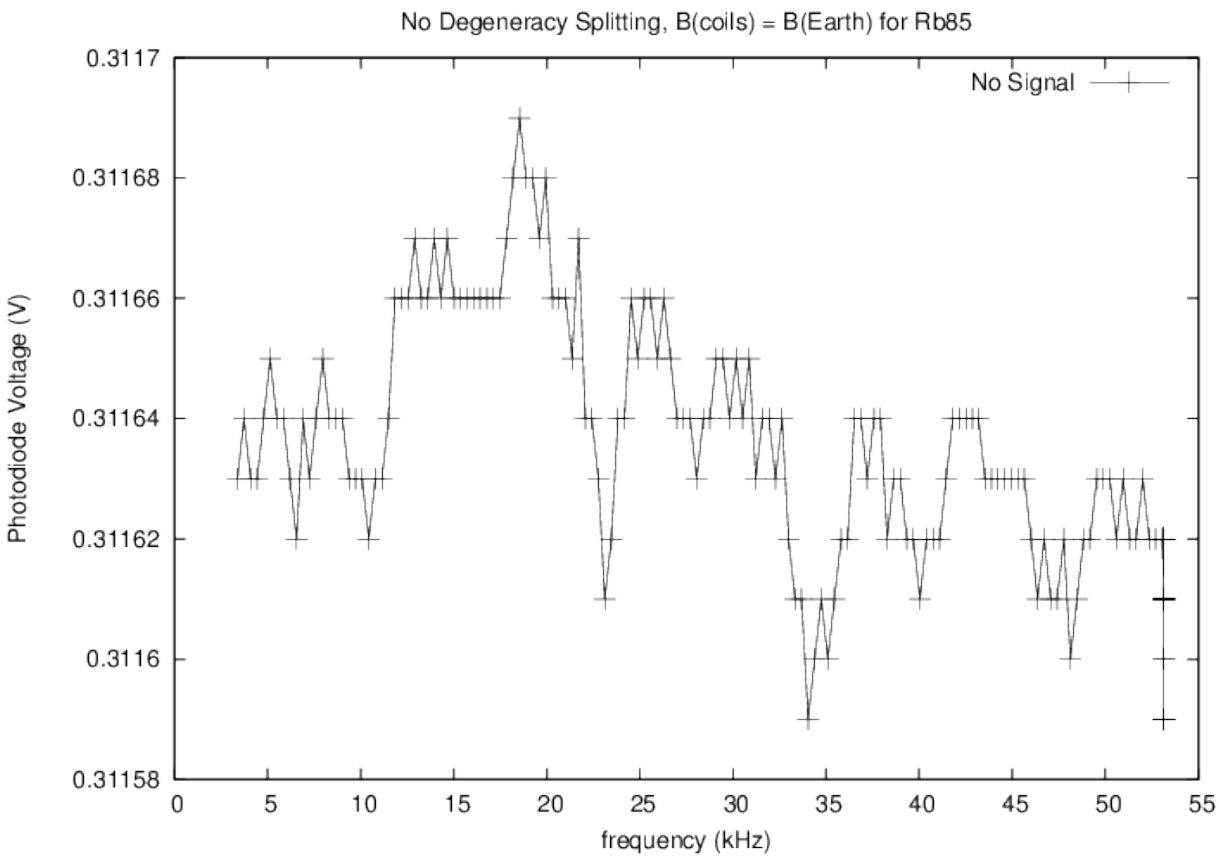

FIG. 10: In ^{85}Rb we found that we could cancel the Earth's magnetic field in a range from $B_{ext} = 41.8919\mu$T $\rightarrow$ 47.98 μT. In this region the signal to noise was so low we could not resolve any absorption dips.

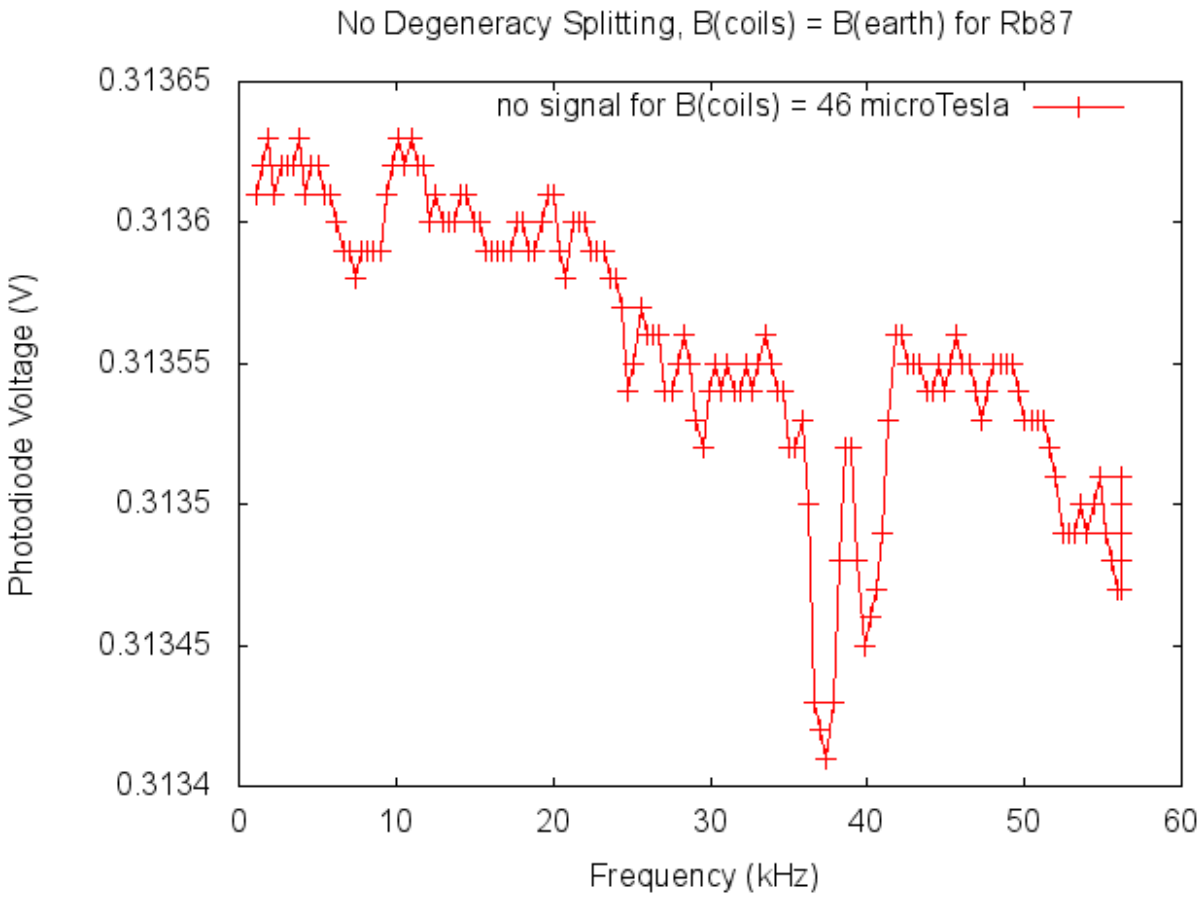

FIG. 11: In ^{87}Rb we found that we could cancel the Earth's magnetic field in a range from $B_{ext} = 41.8919\mu T \rightarrow 48.1632\mu T$. Here is a plot of a frequency sweep within this range. We see the characterisitics of noise, because if we were to repeat the same plot for the same parameters it would look different.

We use this procedure to determine the center frequency as we sweep the magnetic field (scaled from the current) in the *Zeeman effect* region. In doing so we can calculate the Earth's field, when the two isotopes intercept, and find a value for g_F which is given by the slope of the line. The results are as shown.

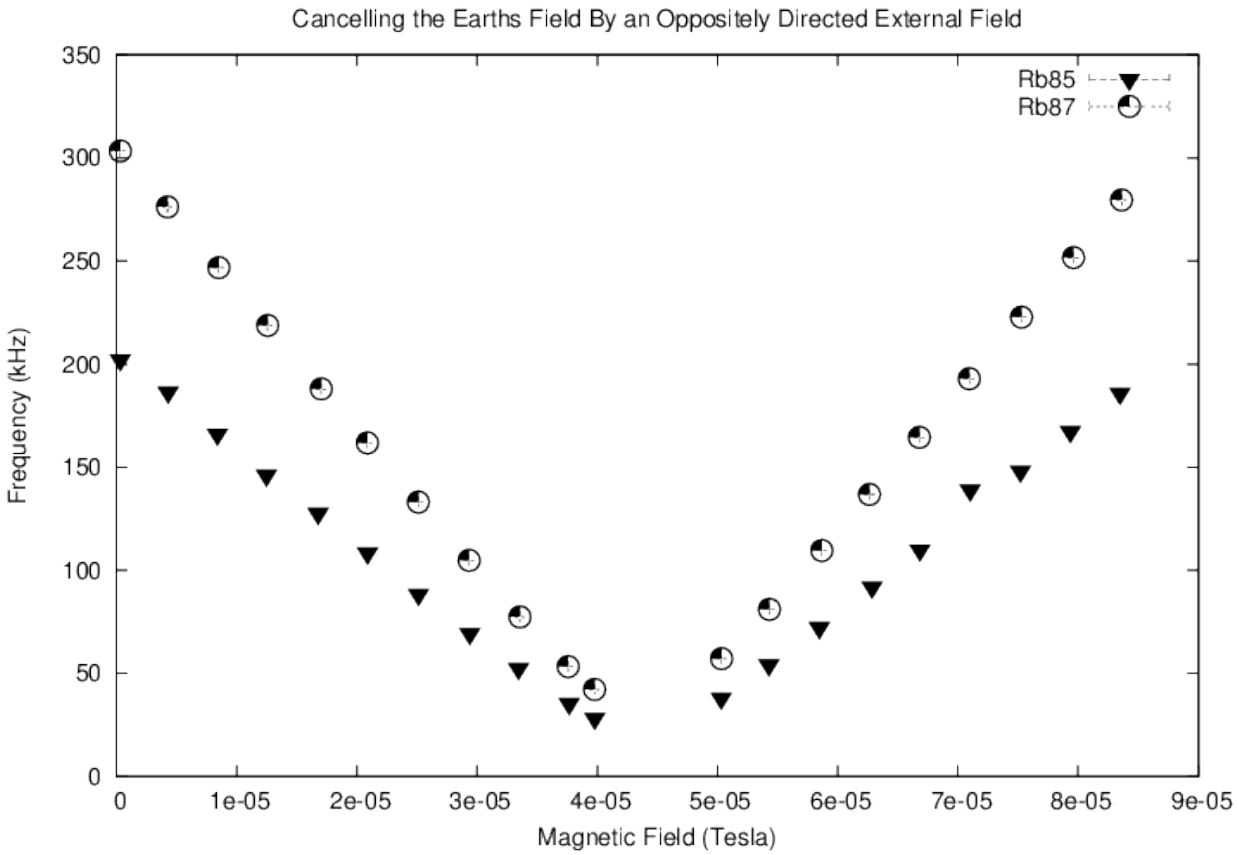

FIG. 12: Here we increased the magnetic field produced by the Maxwell coils to cancel the Earths field. We plot this as a function of the center frequency of absorption. As we expect, as B_{ext} is increased the energy spacing and therefore the frequency between two m_F levels decreases. At a certain point the two fields are of equal magnitude but in opposite directions so they cancel to produce zero magnetic field. Experimentally it was hard to resolve any absorption dips in a certain range of B_{ext} which is why there is a range of no data points. As B_{ext} is increased beyond the magnitude of B_{earth} we see that the frequency increases which is as expected.

For reasons indicated by the figure it was difficult to resolve the energy spacing when $B_{ext} \simeq B_{earth}$. In order to fit an accurate slope to each of these lines for purposes of calculating g_F and the Earths field (intersection of the two lines) we negate all the frequency values before we cancel the Earths field. This should give us the linear relationship shown below. While the graph is completely non-physical (negative frequency) components shown are. It should be noted that we are able to determine g_F from this graph without substracting what the Earths B field from each B_{ext} value which would give B_{tot} because the slope of the line is unchanged. We have shown that g_F is given by,

$$g_F = \frac{h\nu}{\mu_B m_F B_z} \tag{47}$$

Plotting these two lines and using the $y = \alpha * x + b$ to find their slopes, $\alpha \propto g_F$,we find the graphs below.

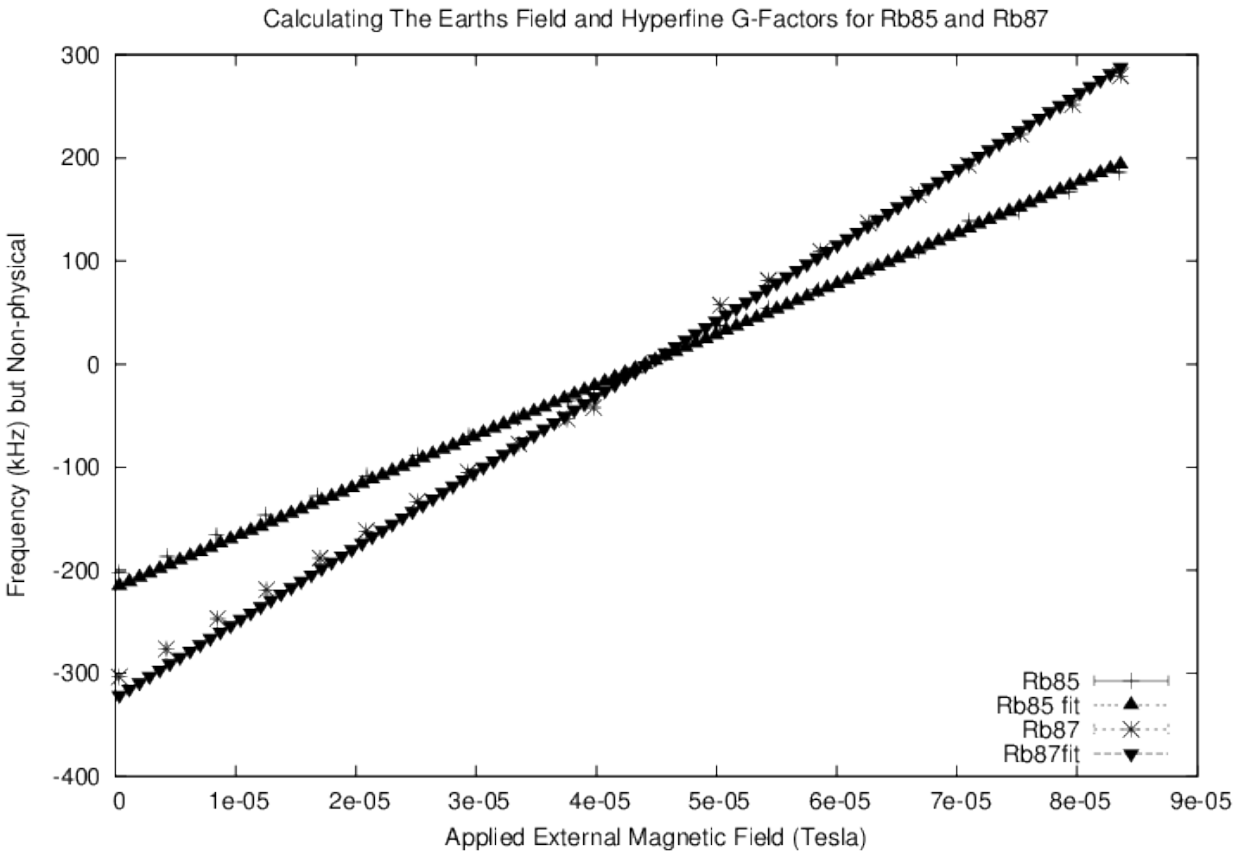

FIG. 13: Although we are plotting negative frequencies (non-physical) we can determine real variables resulting from the fitting functions. We find that the slopes of each line are proportional to the g-factors for the corresponding hyperfine level F. Additionally, the point of intersection between the two lines can be used to determine the Earth's magnetic field.

Below is a table indicating the fitting parameters for each isotope. We use these values to give obtain final measurements of g_F and B_{earth}.

	slope (Hz / T) = α	y-intercept (Hz)	Reduced χ^2
^{85}Rb	$4,906.33 \times 10^6 \pm 1,011 \times 10^5$	$-216,823 \pm 4,472$	0.00824549
^{87}Rb	$7,311.98 \times 10^6 \pm 1,482 \times 10^5$	$-323,253 \pm 6,559$	0.00797794

Using Eq. (47) to include propagation of errors we find

$$g_F = \frac{h\alpha_{^{85}Rb,^{87}Rb}}{\mu_B m_F}\left(1 \pm \frac{\Delta h}{h} + \frac{\Delta\mu_B}{\mu_B} + \frac{\Delta\alpha_{^{85}Rb,^{87}Rb}}{\alpha_{^{85}Rb,^{87}Rb}}\right) \tag{48}$$

where $\alpha_{^{85}Rb,^{87}Rb}$ is the slope corresponding to each isotope shown in the table above. In the ^{85}Rb isotope for F = 3 we measure the g-factor to be $g_F = 0.350(72)$. Comparing this to the theoretical value given in Reference [4] our measurement is different by 5.16%. In the ^{87}Rb isotope for F = 2, the measured g-factor is $g_F = 0.52(15)$. Comparing this to the theoretical value given in Reference [5] our measurement is different by .44%.

Looking back to the fitting functions we can set the two equations of a line equal to each other and solve for the corresponding B value. We find that at the intersection of the two fits, $B_z = B_{earth} = 44.2417 \pm 3.61575\mu T$. Here the error is probably due to not being able to resolve any resonance frequencies near $B_{earth} = B_{coils}$. Other contributions could be ambient magnetic fields that exist in the laboratory as well as placement of many of the metal cabinets and desks. The error does fall within the range of the values of B_{earth} measured in Section 3.2.

3.5. Strong Field Measurements

As discussed in Section 1.5.2 if $|-\vec{\mu}_J \cdot \vec{B}_0| \gg |A(\vec{I}\cdot\vec{J})|$ then the hyperfine energies act as a perturbation to the interaction term. In this regime J and I are good quantum numbers. There becomes a point where the magnetic field is strong enough, as well as the RF power, for us to split the degeneracy such that we can resolve the transition for each Δm_I state for a given m_J value. Theoretical evidence for this is supported in References [4] and [5]. Experimental evidence for this is shown in Figures (16 - 21) and Figures (24 - 30). In the Appendix (Section 7) we present the changes in the absorption dip as we increased the applied magnetic field from the Maxwell coil. In this case we reversed the polarity of the current such that the magnetic field from the Maxwell coil B_{ext} adds to the Earth's field B_{earth} which we have calculated to be $44.2417 \pm 3.61575\mu T$ in the section above. In the Appendix we show the splittings in this region for both isotopes.

As shown that we begin to resolve the transitions between each magnetic sublevel $\Delta m_I = -1$. In the case of ^{87}Rb we believe we observed two photon transitions where $\Delta m_I = -2$. At this strong field, the splitting between m_I levels is large and equivalently our RF power is high too. Therefore once an electron deexcites to a lower m_I level instead of being optically pumped to the $5p^2P_{1/2}$ state it can undergo another magnetic resonance transition to the next lower m_I level

making $m_I(final) = m_I(initial) - 2$ in this simplified three level system. For ^{85}Rb I = 5/2, $m_J = +1/2, -1/2$ and $m_I = -5/2, -3/2, -1/2, +1/2, +3/2, +5/2$ which corresponds to a total of 5 possible transitions. For $m_J = +1/2$ the states where $m_I > 0$ have a higher energy then states where $m_I < 0$. This phenomena is opposite when $m_J = 1/2$, $m_I < 0$ states have higher energy than $m_I > 0$ states. In the case of ^{87}Rb I = 3/2, $m_J = +1/2, -1/2$ and $m_I = -3/2, -1/2, +1/2, +3/2$ making a total of 3 possible transitions. We observe the same phenomena where for $m_J = 1/2$ the states when $m_I > 0$ have a greater energy than $m_I < 0$ states. The opposite is true for $m_J = -1/2$.

For the ^{85}Rb isotope, I = 5/2, we obtain results we would expect in terms of the number of absorption dips. These corresponding to the possible values of $m_I = +5/2, +3/2, +1/2, -1/2, -3/2, -5/2$ making a total of five possible transitions. As shown in the graph we expect the $+5/2 \rightarrow +3/2$ transition to be the strongest signal, at the lowest energy, with each lower transition decreasing in signal strength but increasing in energy separation. We also observe some unusual phenomena shown by the presence of a sixth absorption dip. This transition could possibly be from $m_J = 1/2, m_I = -5/2$ to $m_J = -1/2, m_I = -5/2$. There is room to be skeptical of this explanation by looking at Figure 4 in Reference [4]. We expect the energy gap between $m_I = -5/2$ in $m_J = +1/2$ and $m_J = -1/2$ to increase as the total magnetic field increase but in our measurements the energy separation between dips trends to be even. Even if we were at such a strong field where the energy separation between m_I levels increases linearly, the energy gap between $m_I = -5/2$ for $m_J = +1/2 \rightarrow m_J = -1/2$ should be much larger than the gap between $m_I = -3/2 \rightarrow -5/2$ for $m_J = +1/2$. We find the energy separation to be nearly even.

For the ^{87}Rb isotope, I = 3/2, we obtain similar results. The number of expected absorption dips (3) is present. This corresponds to the change in $m_I : +3/2 \rightarrow +1/2, +1/2 \rightarrow -1/2, -1/2 \rightarrow -3/2$. Again since we optically pump to the $m_I = +3/2$ state we expect the $+3/2 \rightarrow +1/2$ to be the strongest transition but also occur at a lower energy, Figure 4 in Reference [5], which is observed experimentally. As with the other isotope we observe extra dips that we do not expect. We cannot explain the second dip seen in Fig. (22). As we increase the B field and observe additional dips the same reasoning can be applied as discussed above. This would mean that transitions are being made between $m_I = -3/2$ for $m_J = +1/2$ to $m_J = -1/2$ states. Again we are very skeptical of these results for the same reasons as discussed above by comparing our results to Reference [5].

In addition, we observe what we believe to be mutliphoton transitions seen to first appear in Fig. (28) and shown completely in Fig. (29). There is no other explanation for these dips to arise and the fact that the growth in between two resonance dips corresponding to two different transitions gives indications that this is the case. It is unusual is that these dips disappear in the

next graph which corresponds to a higher magnetic field. A way to resolve this would be if the separation between the two transitions $1 \rightarrow 2, 2 \rightarrow 3$ becomes too large for the present RF power to make excitations between $1 \rightarrow 3$.

4. CONCLUSION

This experiment demonstrates the application of optical pumping used to prepare states for magnetic resonance. We have shown that electrons can be pumped to a dark state but utilizing σ^+ polarization. Spin resonance, induced by a radio frequency signal, can stimulate transitions between magnetic sublevels which can be summarized in the picture of a two-level system. My measuring the frequency at which these transitions occur the values of physical constants such as the Landeé g-factor and the Earth's magnetic field can be obtained.

5. ACKNOWLEDGEMENTS

I would like to thank Dr. Schneble and Ludwig Krinner for their assistance in teaching us the theoretical concepts behind this experiment and for providing multiple references used in this write-up. I would like to thank Dr. Metcalf and John Elgin for helping me with questions pertaining to the experiment. I would also like to thank Mehdi Namaz for his help in the laboratory.

6. REFERENCES

1. Bloom, Arnold L. **Optical Pumping**. *Scientific American, Inc.* 1960.

2. PHY 445 **Optical Pumping**. 2013

3. Schneble, Dominik. **Ultracold Atomic Physics**. *PHY 565 Quantum Electronics* Spring 2012.

4. Steck, Daniel Adam. **Rubidium 85 D Line Data**. *Oregon Center for Optics and Department of Phyiscs, University of Oregon.*

5. Steck, Daniel Adam. **Rubidium 87 D Line Data**. *Oregon Center for Optics and Department of Phyiscs, University of Oregon.*

6. Griffiths, David. J. **Introduction to Quantum Mechanics**. *Pearson Education, Inc.* 2005.

7. NIST Reference on Constants, Units, and Uncertainty. **http://physics.nist.gov/cgi-bin/cuu/Value?gem**. *National Institute for Standards and Technology.* June 2011

8. Milonni, Peter W. & Eberly, Joseph H. **Laser Physics**. *Wiley* 2010.

7. APPENDIX

Here we show the transformation of the absorption dip as we increase the applied field in the strong field regime. The following graphs show the effects of increasing the current, a larger B field, causes a higher energy separation between magnetic sublevels. All these graphs are for the strong field regime where the hyperfine structure is a perturbation to the applied field. It is shown that we begin to resolve the transitions between each magnetic sublevel $\Delta m_I = -1$.

The following graphs are for the ^{85}Rb isotope for an increasing current. The corresponding B field is noted in the caption which includes B_{earth} using the value calculated in Section 3.4.

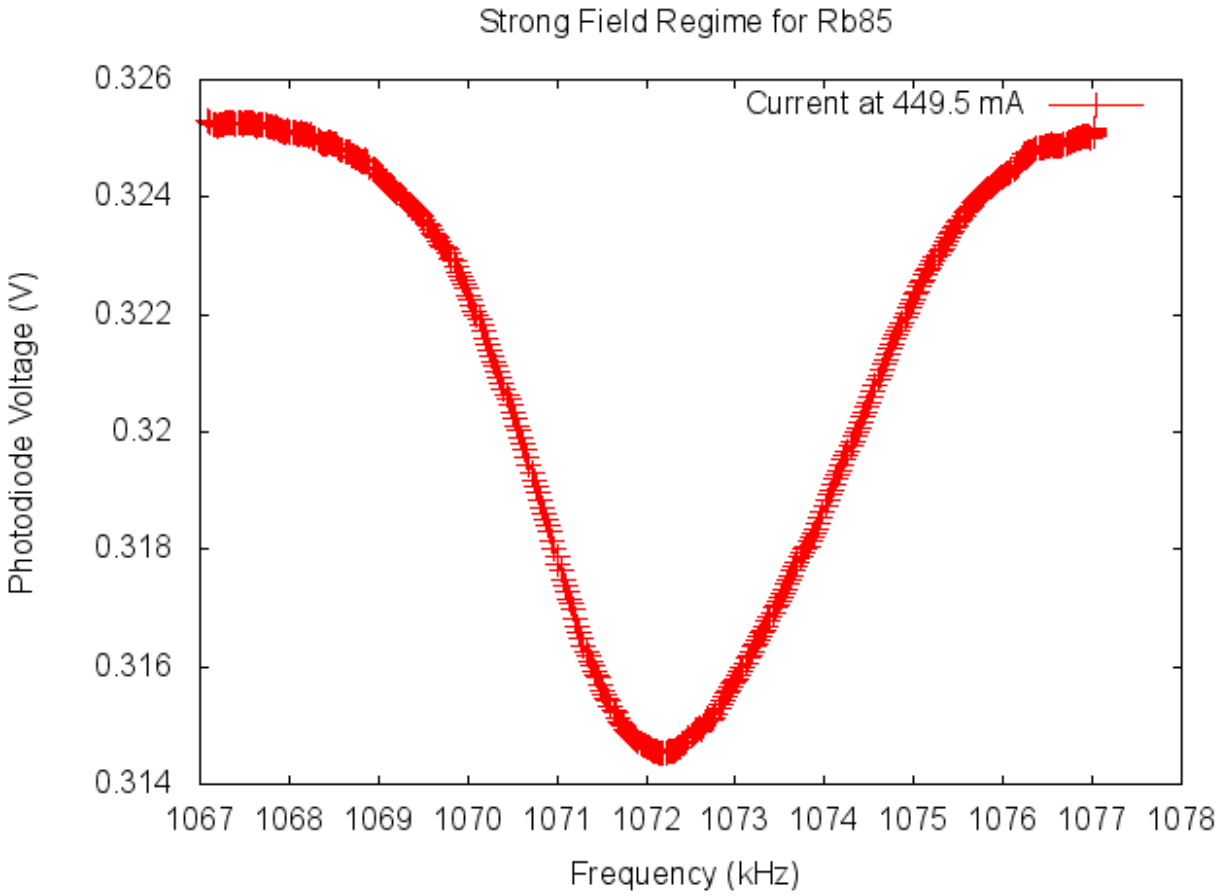

FIG. 14: For $B = 231.796 \pm 3.6157 \mu T$ we have an energy spacing of approximately 1072.2 kHz.

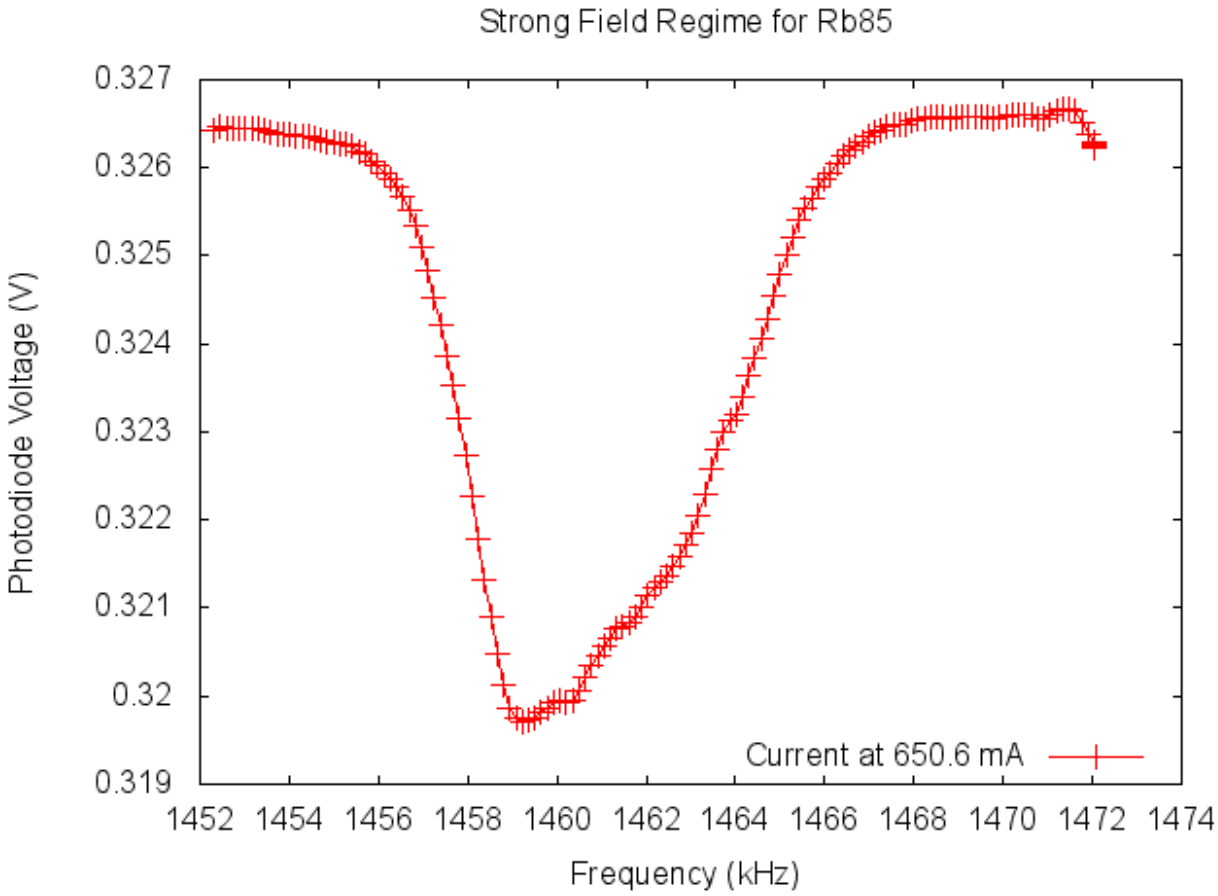

FIG. 15: For $B = 271.463 \pm 3.6157 \mu T$ we have a main dip around 1459 kHz. Here we begin to see multiple dips seperating themselves from main dip. This corresponds to the separation between m_I states beginning to be resolvable.

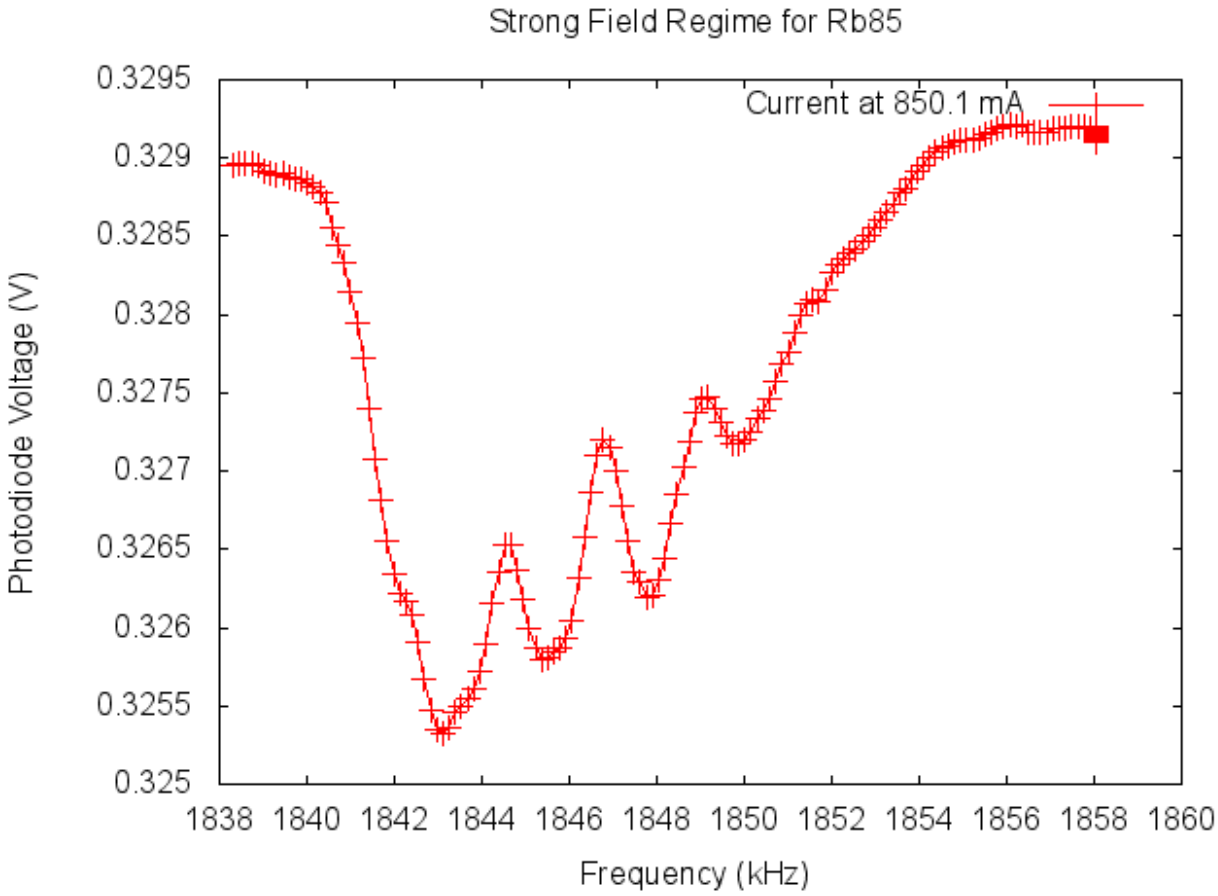

FIG. 16: For $B = 398.946 \pm 3.6157 \mu T$ the main dip resides around 1842 kHz. The splittings between lower m_I states are shown to be approximately 1845.8, 1848, and 1855 kHz respectively. Each weaker dip at a higher energy indicates electrons going from one lower m_I state to the one below it.

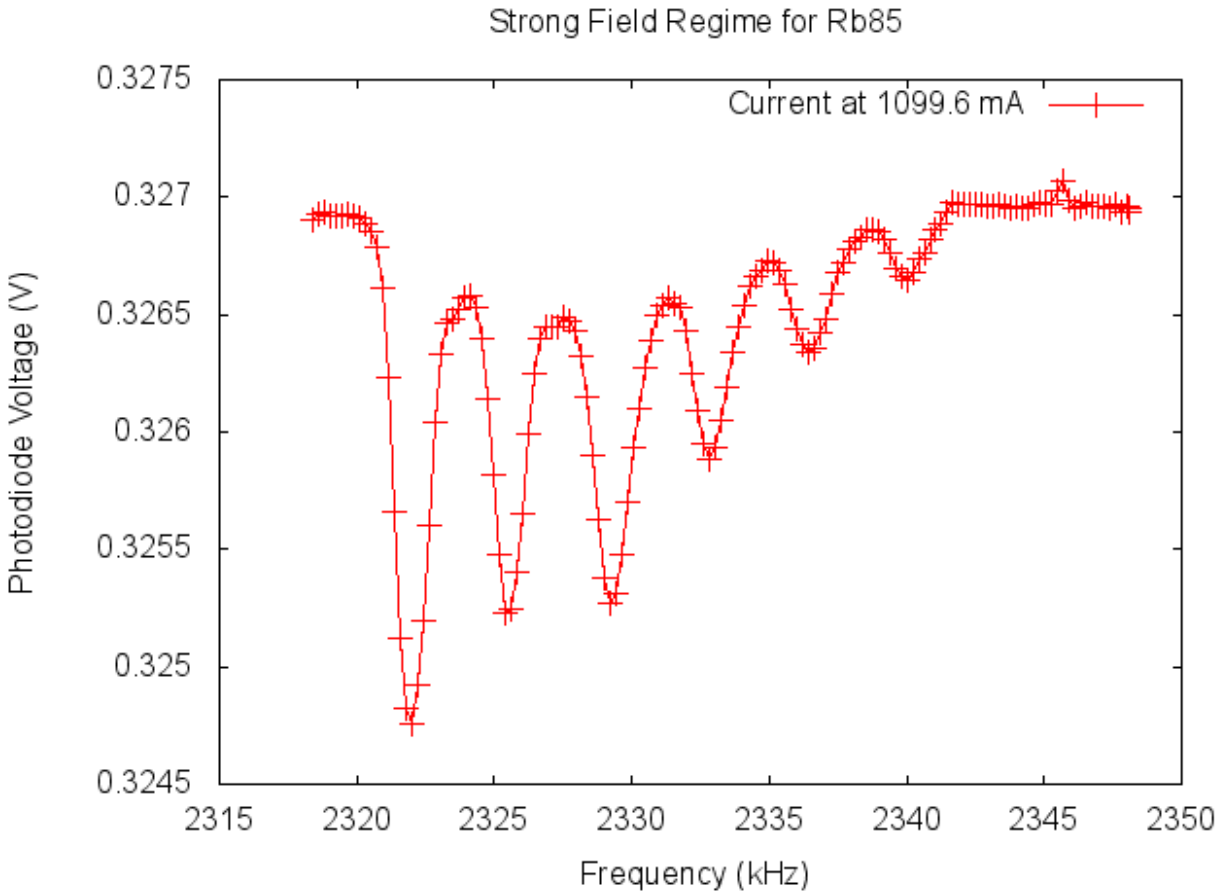

FIG. 17: For $B = 458.808 \pm 3.6157\mu T$ the presence of transitions between m_I states are apparent. The center frequencies for each dip are located at approximately 2322, 2326 2329, 2332.5, and 2337 kHz. We also notice an unexpected dip at 2341 kHz.

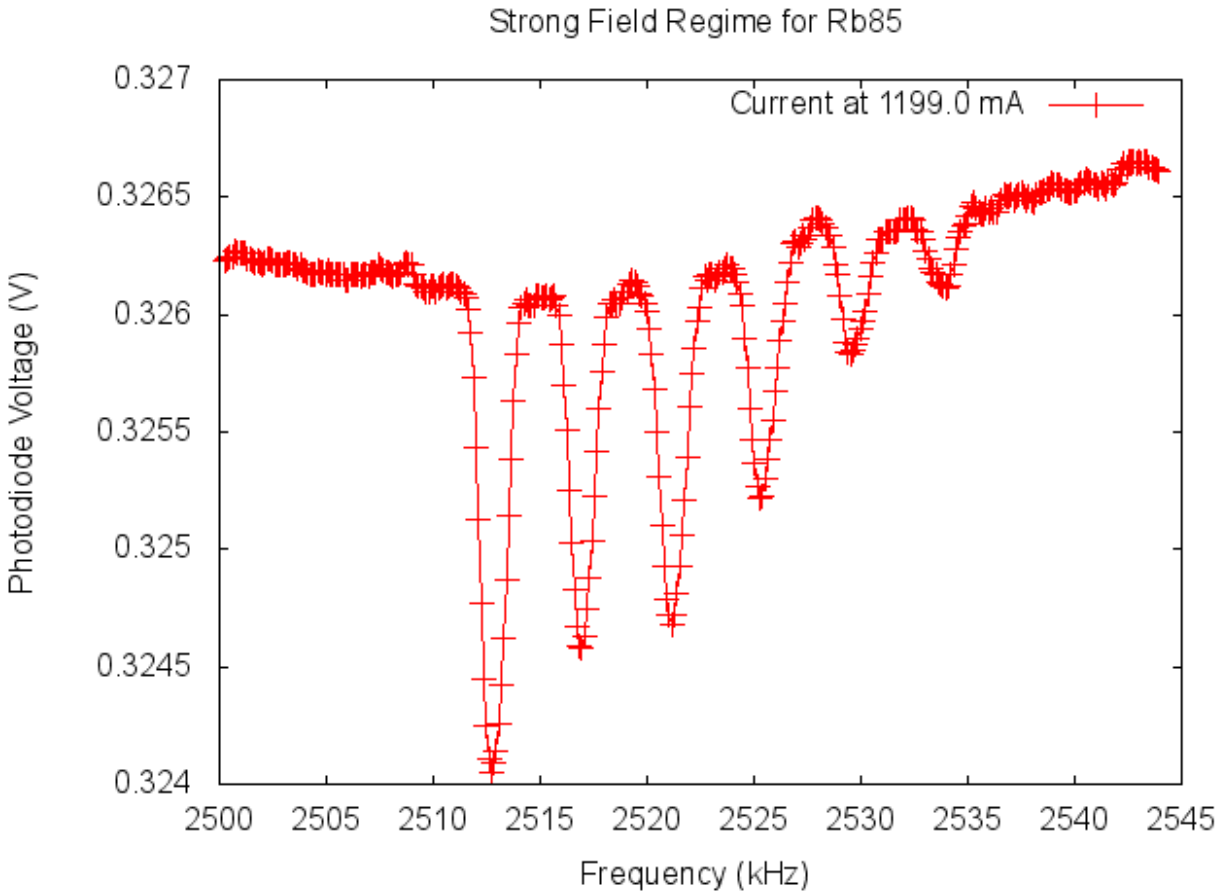

FIG. 18: For $B = 544.524 \pm 3.6157\mu T$ we find our transitions occur at approximately 2512.5, 2517, 2522, 2526, 2529 kHz with the unexpected dip at 2534 kHz respectively.

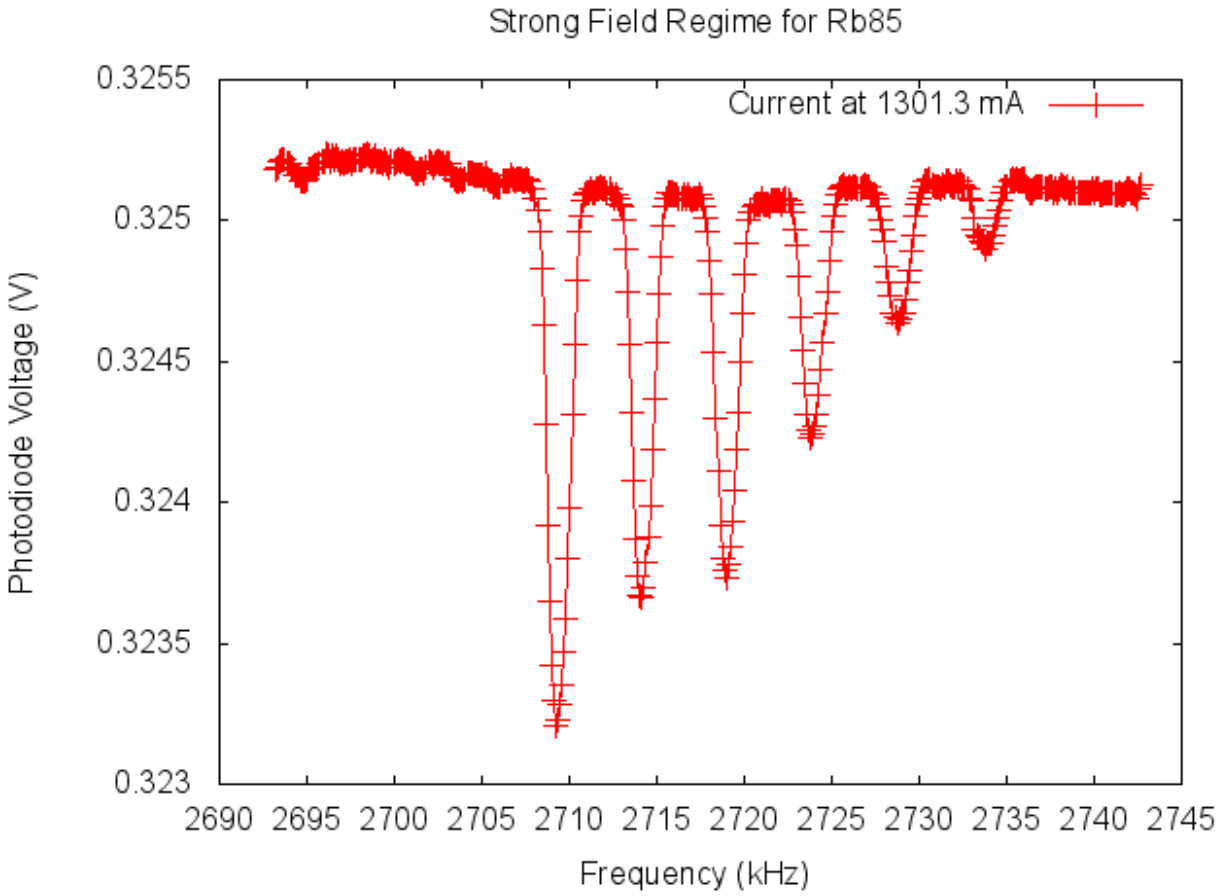

FIG. 19: For $B = 587.209 \pm 3.6157 \mu T$ we observe several clean transitions. These transitions are centered at approximately 2709, 2714, 2718.5, 2725, 2730, and 2733 kHz respectively. As we suspect the energy gap betwen the same m_I states is increasing for increaseing B-field. The presence of the extra sixth dip, here at 2735 kHz is still evident.

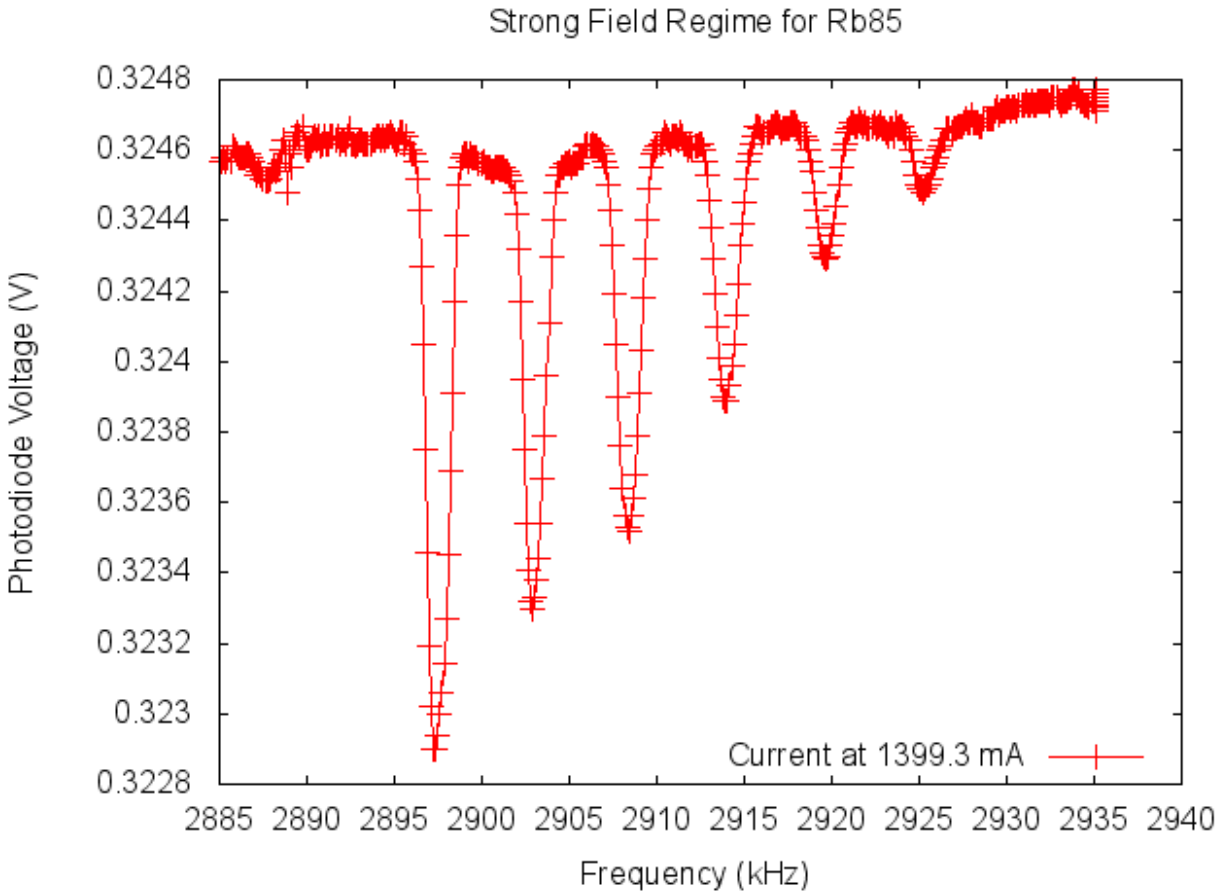

FIG. 20: For $B = 628.1 \pm 3.6157 \mu T$ these transitions corresponding to $m_I^{'} = m_I - 1$ down to the lowest m_I level for that specific hyperfine structure. It makes sense that the weakest signal is the least probable corresponding to $m_I^{'} = -m_I$ not considering the weakest dip here which is unexpected.

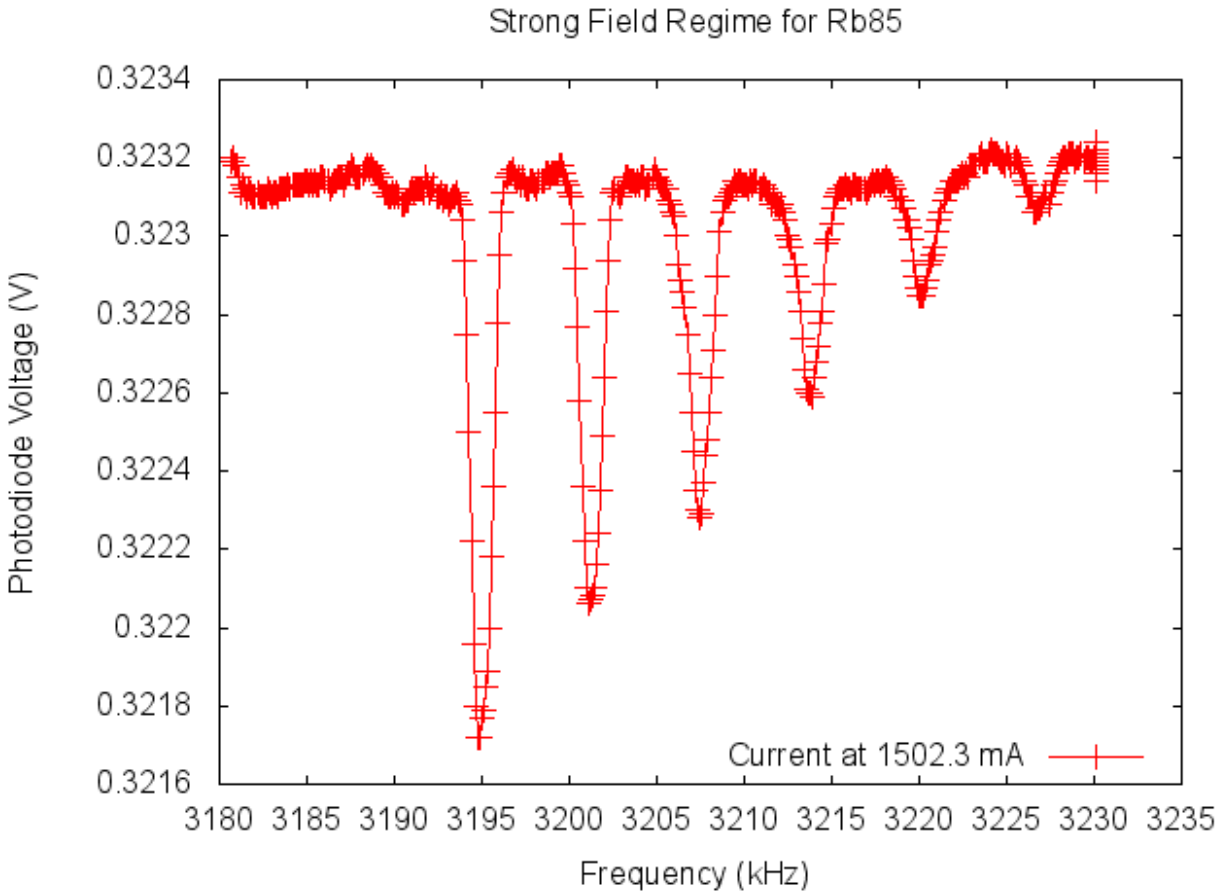

FIG. 21: For $B = 671.076 \pm 3.6157 \mu T$ we continue to see several transitions between m_I states as expected. Additionally the energy spacing between them increases as well. Here the dips are centered at 3195, 3202, 3207.5, 3213.5, 3221, and 3227.5 kHz approximately. It is reassuring the number of dips expected is consistent in our measurements once they were all resolved. This, of course, does not include the dip at 3227.5 kHz which we have possible suspicions for.

The following graphs are for the ^{87}Rb isotope for an increasing current. Recall, in ^{87}Rb I $= 3/2$ and therefore $m_I = -3/2, -1/2, +1/2, +3/2$. So once this is resolved we should see a total of 4 possible transitions. The corresponding B field is noted in the caption.

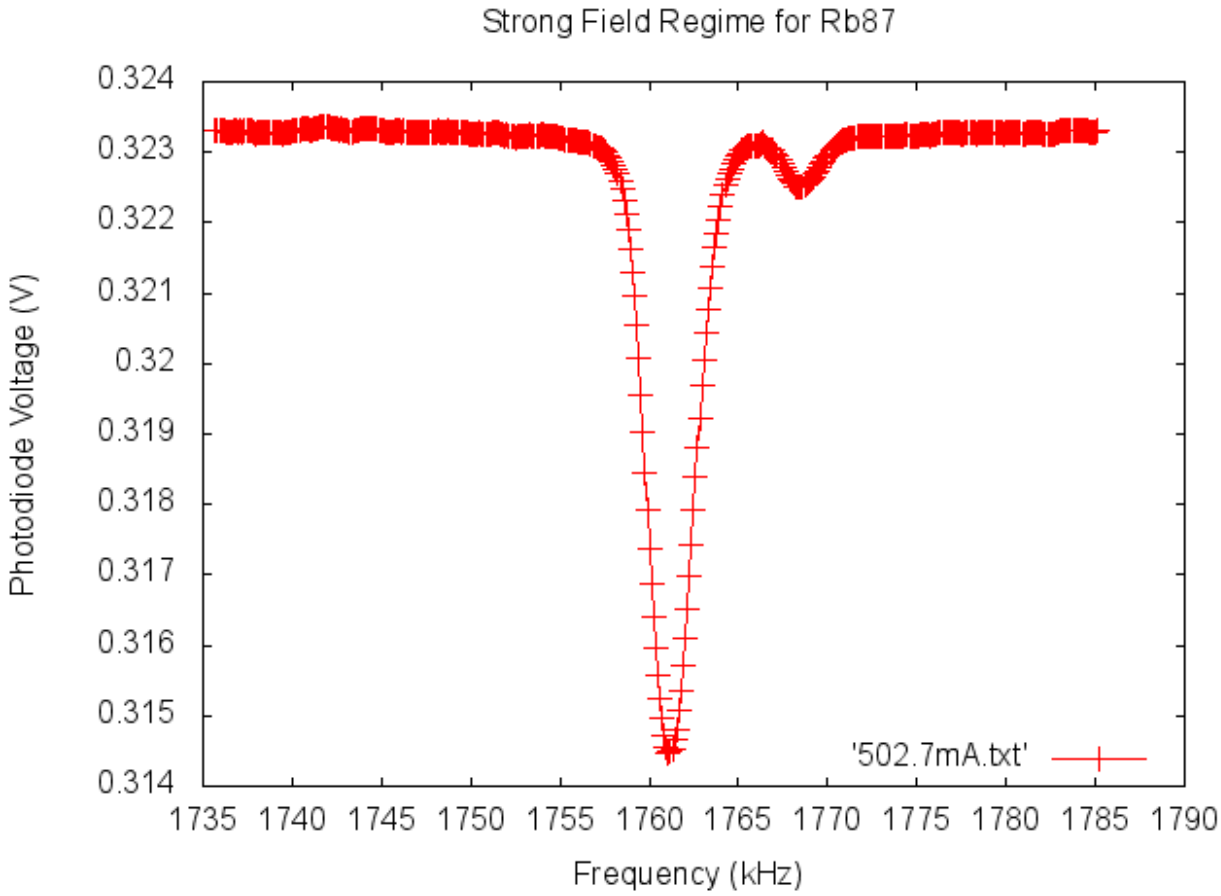

FIG. 22: For $B = 253.993 \pm 3.6157 \mu T$ we have our characteristic absorption dip for $\Delta m_I = -1$. The side dip is a result of some unkown phenomena probably related to the apparatus and not the atomic structure. As we cannot resolve over m_I transitions I do not believe this is a mutliphoton transition, $\Delta m_I < 1$

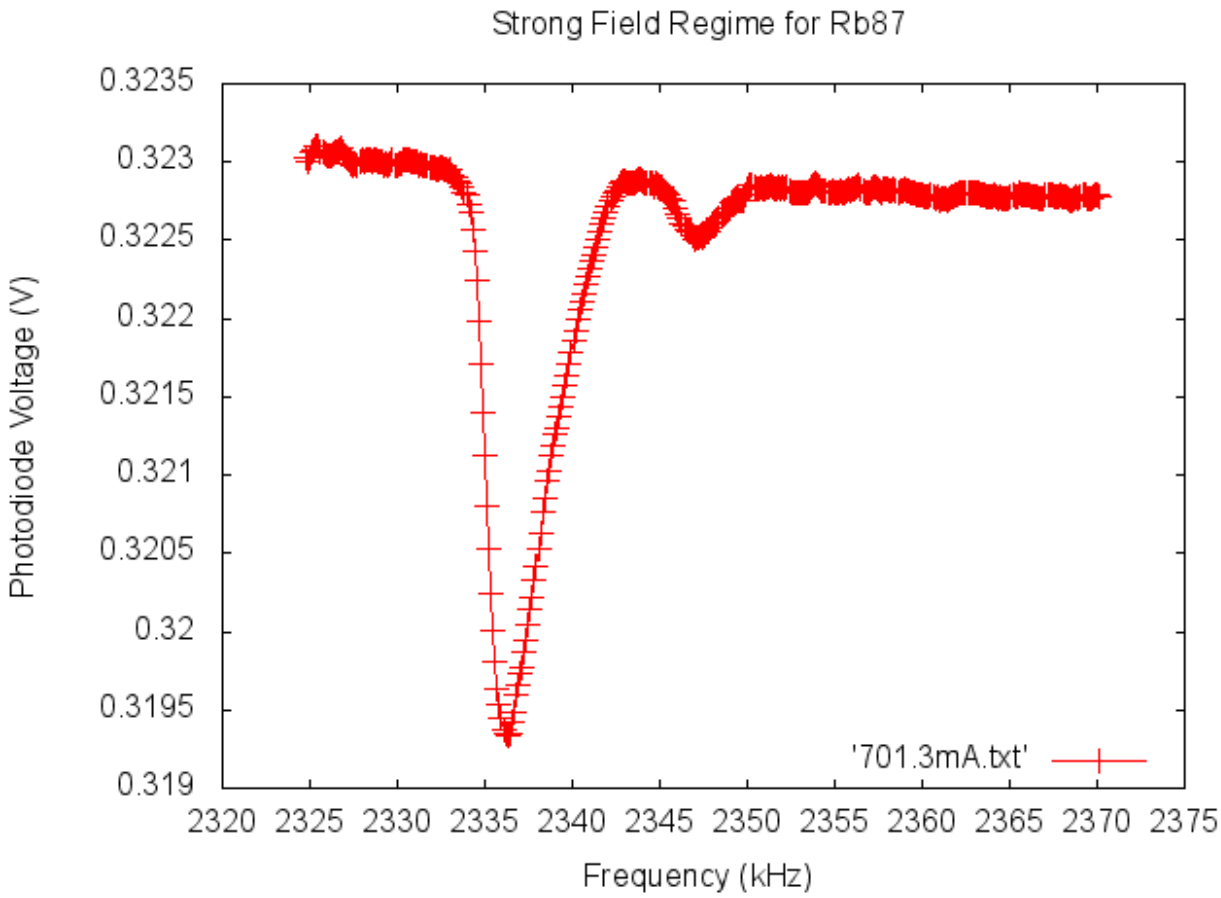

FIG. 23: For $B = 336.859 \pm 3.6157 \mu T$ we begin to see the dip become asymmetric as the other transitions begin to seperate from the main dip.

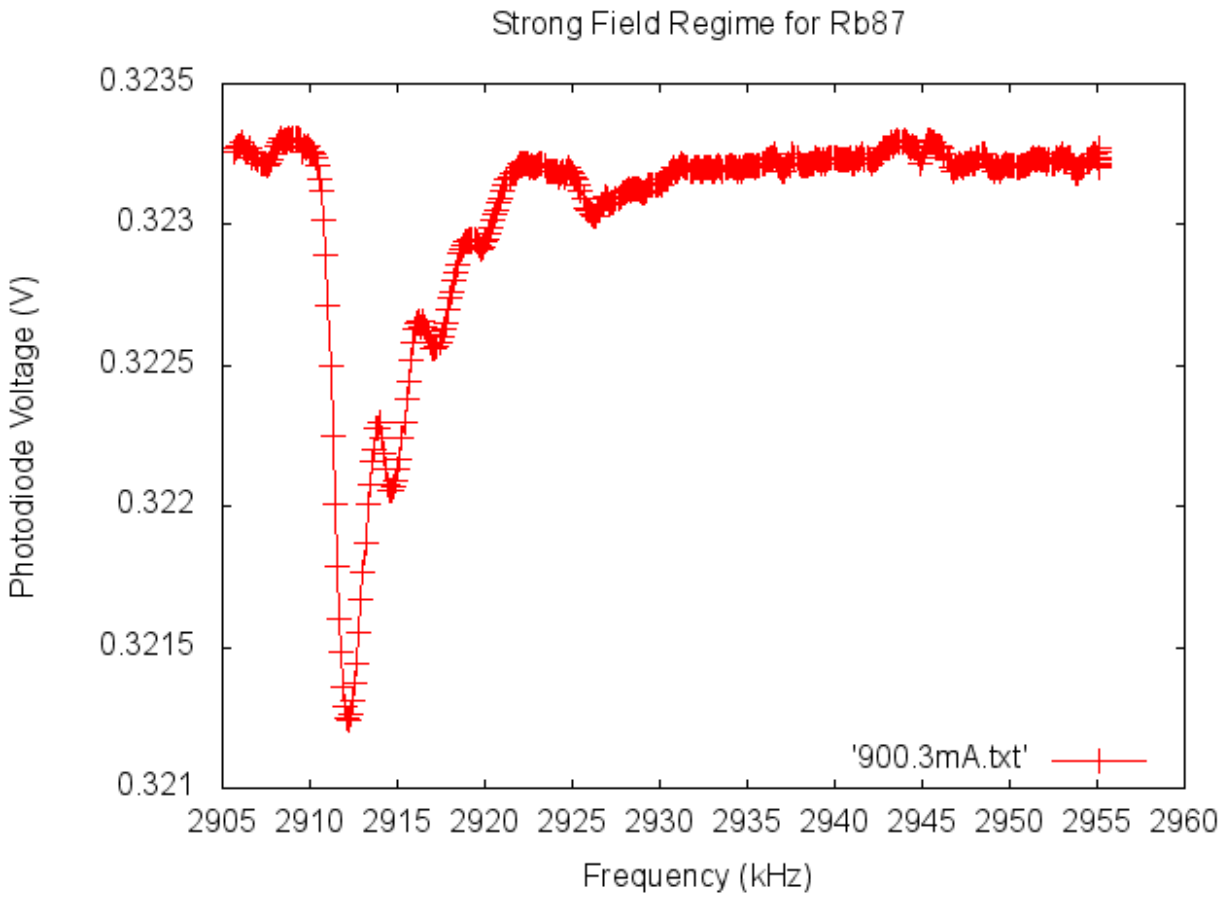

FIG. 24: For $B = 419.892 \pm 3.6157 \mu T$ it is clear that other m_I transitions have a large enough energy gap to begin to differentiate themselves.

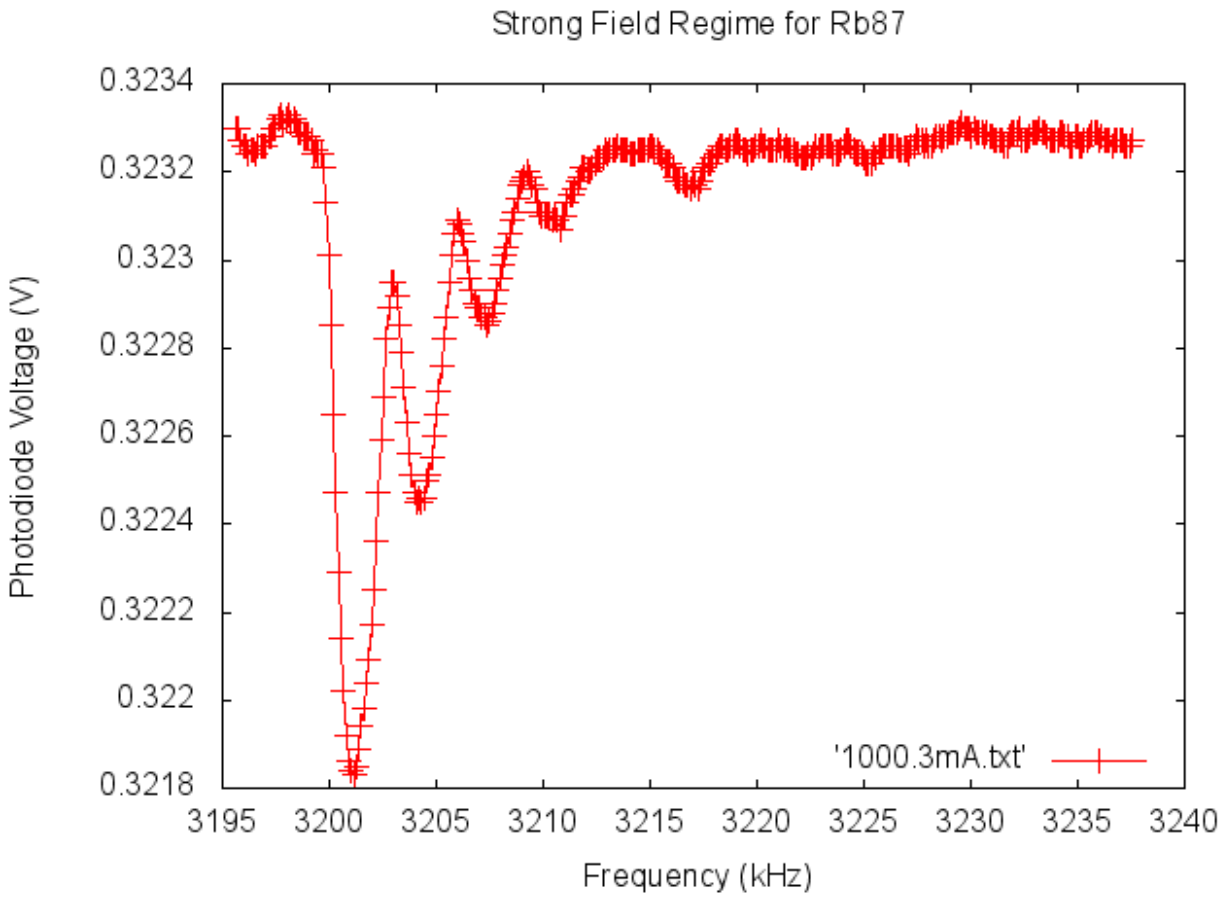

FIG. 25: For $B = 461.617 \pm 3.6157 \mu T$ the signal strength from these other transitions increase and showcase their center frequencies which are 3201.5, 3205, 3207.5 3210 kHz approximately. As expected we have three transitions present, neglecting the two unknown dips to the right of them all.

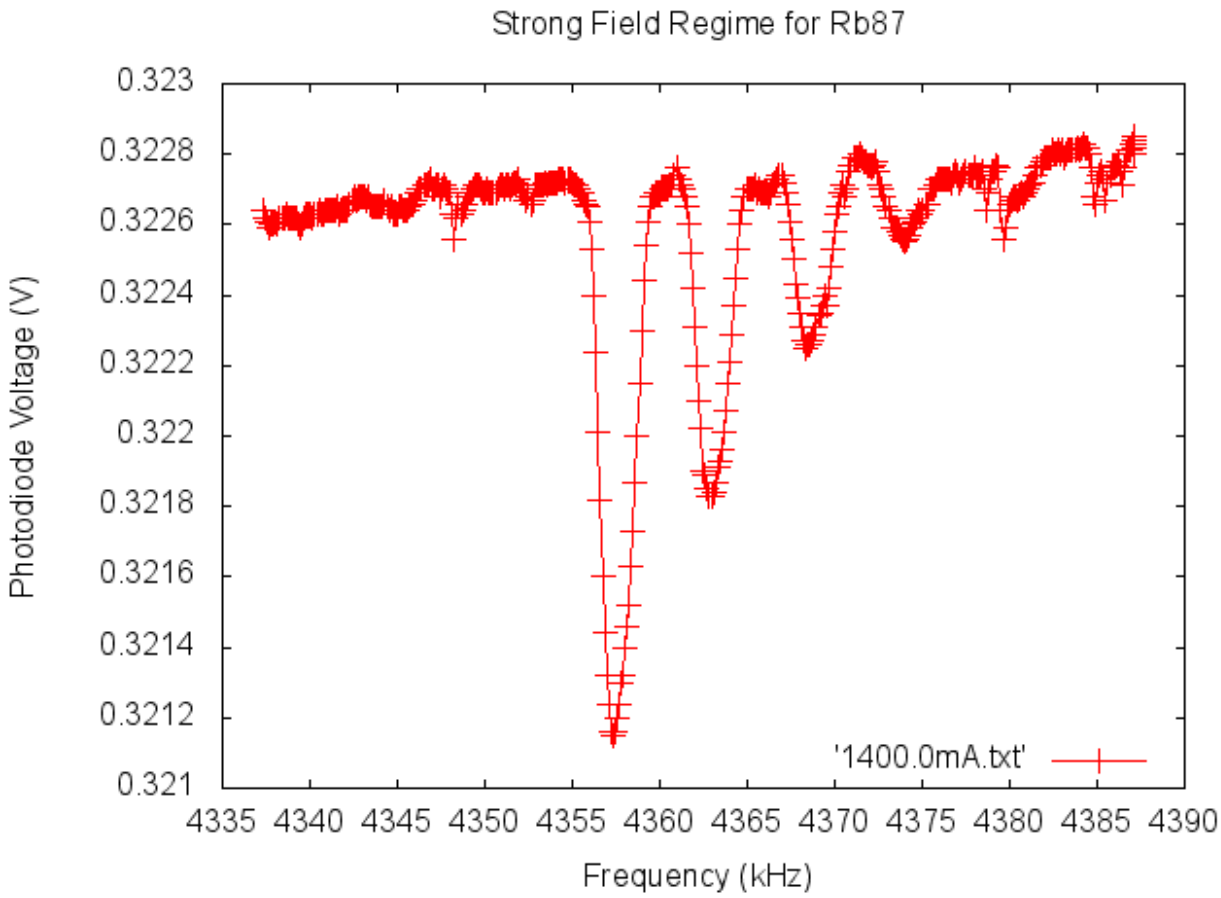

FIG. 26: For $B = 628.392 \pm 3.6157\mu T$ the transitions now have their own linewidth because the magnetic field is strong enough to split these state enough in terms of energy to resolve their full shape.

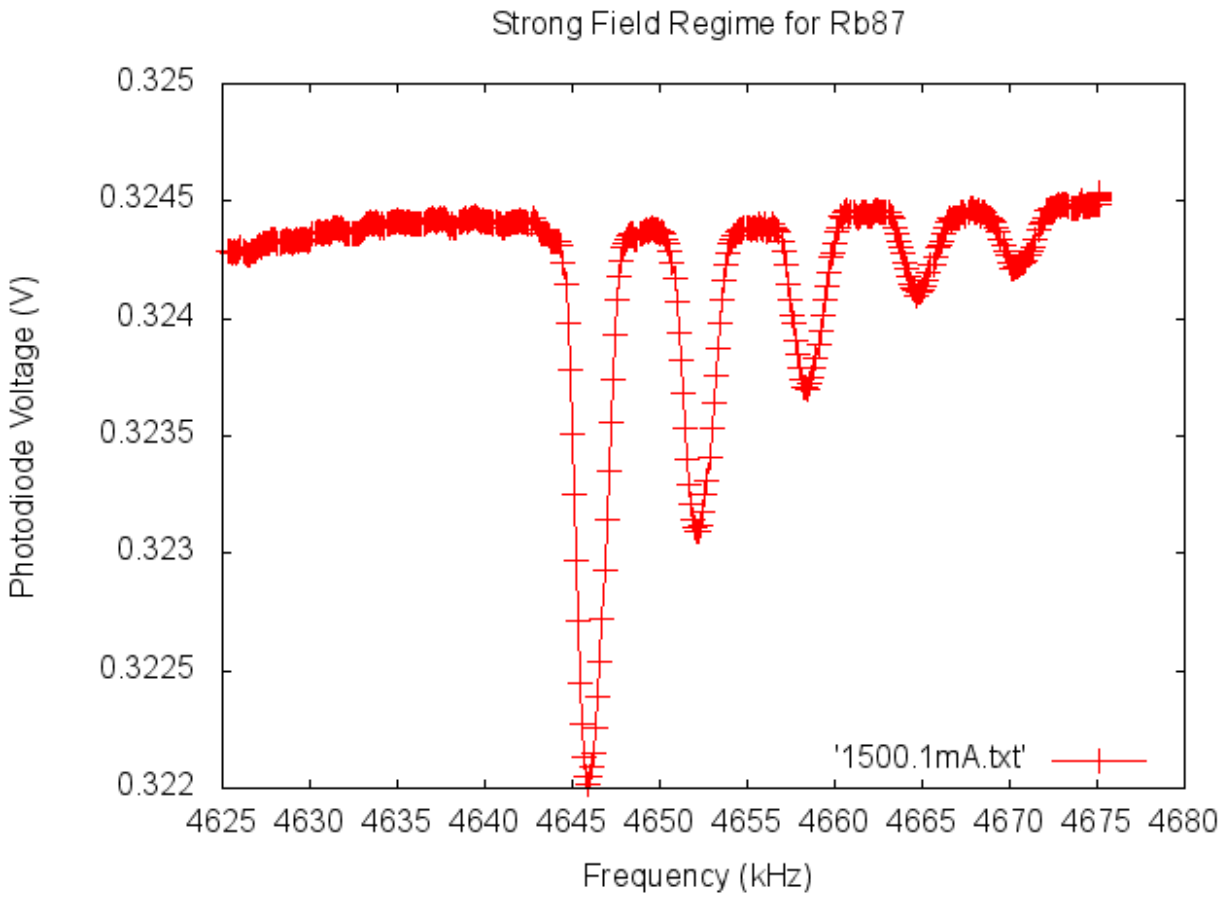

FIG. 27: For $B = 670.158 \pm 3.6157 \mu T$ the lineshape for each of these transitions has become really clean. The presence of the abnormal fourth and fifth dip to the right is still present and has been for each step in B.

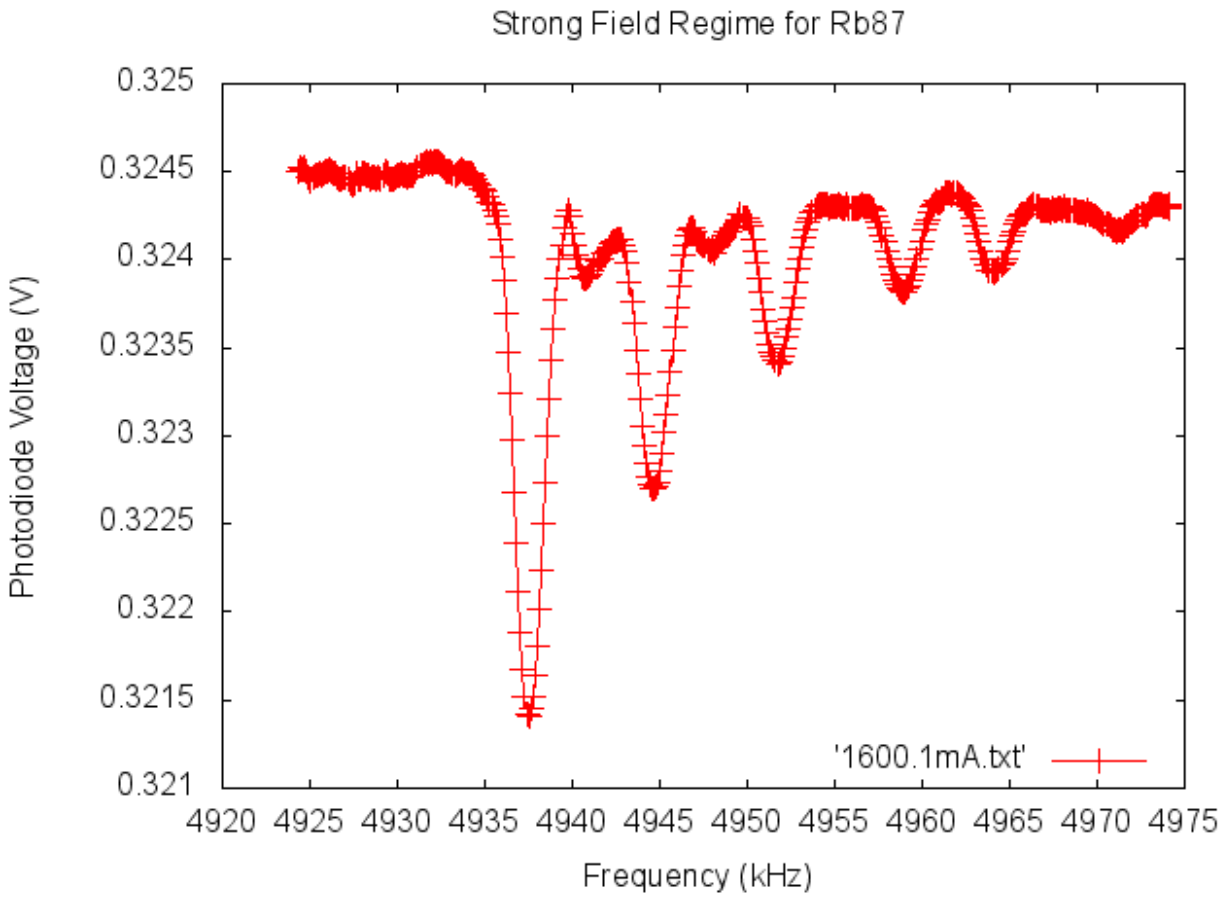

FIG. 28: For $B = 711.883 \pm 3.6157 \mu T$ we begin to see the arisal of multi-photon transitions where $\Delta m_I > 1$ meaning that an electron can deexcite from $m_I = +3/2$ to 0. It makes sense that their dips arise in between the two since the frequency should be roughly the average of the two.

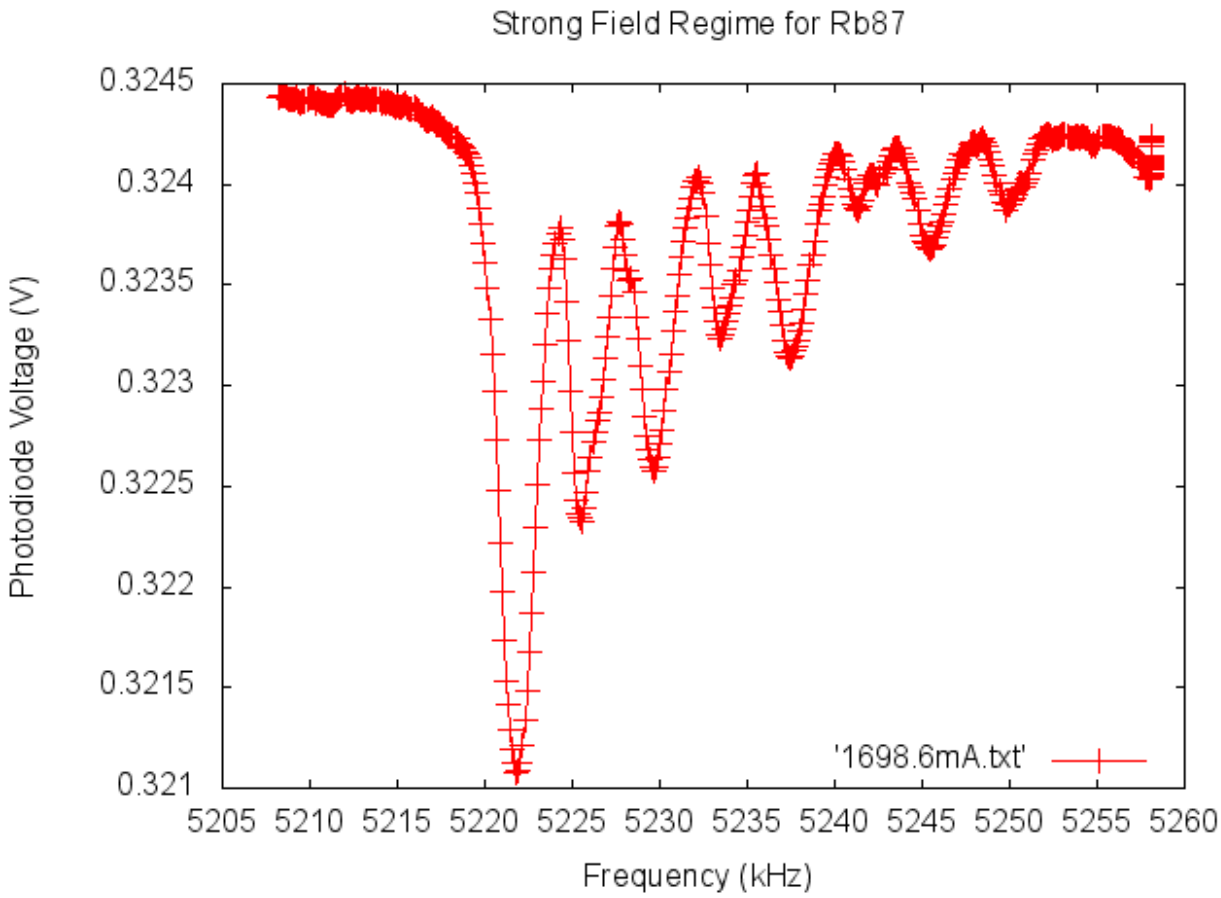

FIG. 29: For $B = 752.983 \pm 3.6157 \mu T$ the multiphoton transitions have become very prominent and well defined. I cite the arisal of these extra dips as multiphoton transitions because of their center frequency and the number of them

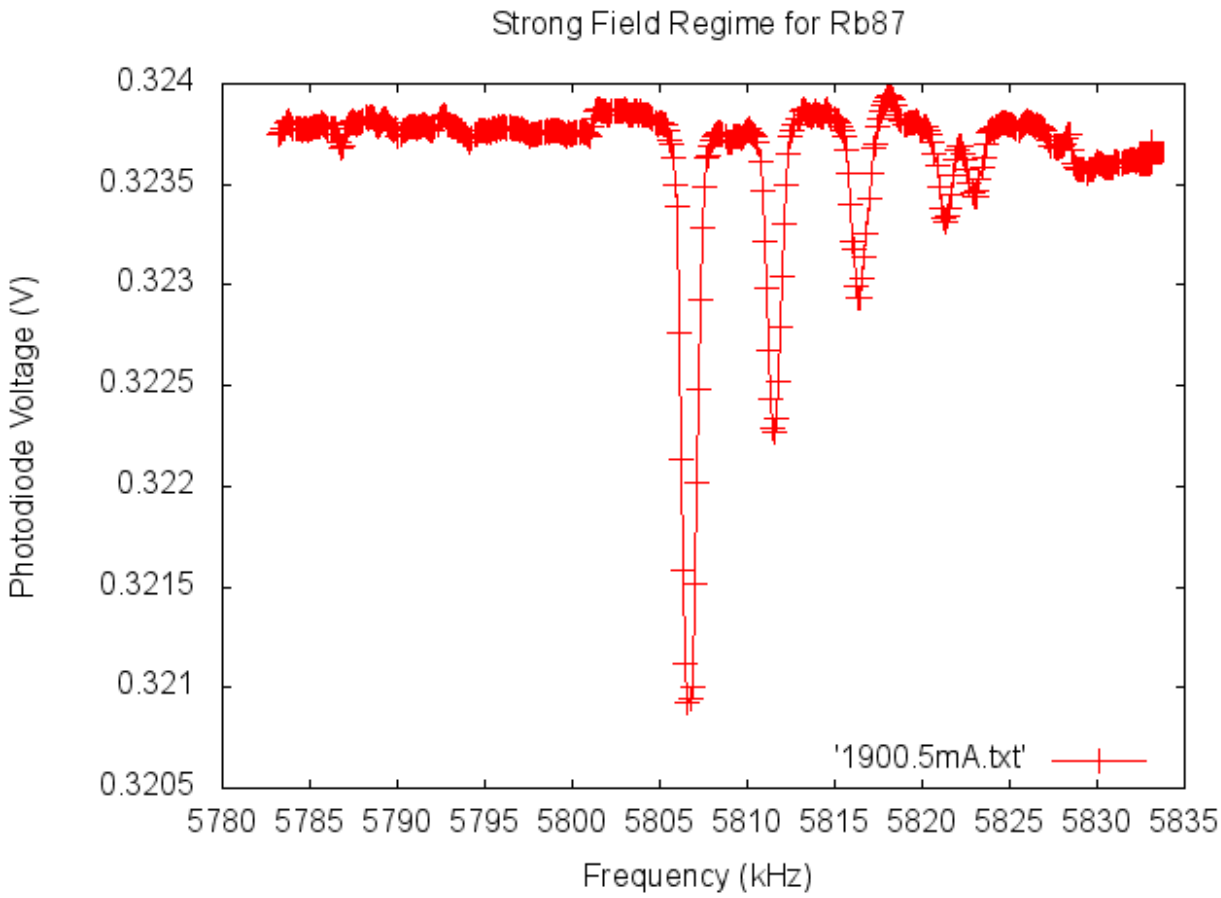

FIG. 30: For $B = 837.225 \pm 3.6157 \mu T$ we need to sweep over such a large range the absorption dips begin to appear thin. The multiphoton transitions that were present in the previous graph are not now which is very interesting. This could be to the power of the RF not being strong enough to resolve the transitions.